

photochemistry of the *unprotonated* 9-*cis* and 11-*cis* Schiff bases, indicating that either a polar or hydrogen-bonding environment must be provided for the chromophore for efficient isomerization. A good deal of experimental evidence suggests, however, that the chromophore in rhodopsin is protonated.<sup>3</sup> Importantly, our results for the *protonated* 9-*cis*, 11-*cis*, or 13-*cis* Schiff bases demonstrate that only the 11-*cis* isomer efficiently isomerizes,  $\geq 5$  times more efficiently than the 9-*cis* (or 13-*cis*) isomer. For parallel natural occurring systems, experimental evidence for rhodopsin (11-*cis*) shows that the quantum yield of conversion to bathorhodopsin (all-*trans*) is  $\sim 7$  times greater than of isorhodopsin (9-*cis*) to bathorhodopsin for vertebrate pigments and 4 times greater for invertebrate pigments.<sup>38</sup> Note that our ratio of 5 times greater

for the models is within this latter range of 4-7. Thus, our results provide insight into why the 11-*cis* isomer is the one naturally found in the visual pigment.

Recent results on poly(ethylene glycol) oligopeptide Schiff bases of 11-*cis*-retinal show a  $\phi$  value as high as 0.37.<sup>39</sup>

**Acknowledgment.** The laser-flash experiments were performed at the Center for Fast Kinetics Research at the University of Texas at Austin, which is supported by NIH Grant RR-00886, the Biotechnology Branch of Research Resources, and the University of Texas. We thank Hoffman-LaRoche for their gifts of some of the retinal isomers.

(37) Spalink, J.; Reynolds, A.; Rentzepis, P.; Sperling, W.; Applebury, M. *Proc. Natl. Acad. Sci. U.S.A.* **1983**, *80*, 1887.

(38) Suzuki, T.; Callender, R. *Biophys. J.* **1981**, *34*, 261.

(39) Freedman, K.; Becker, R. S.; Hannak, D.; Bayer, E. *Photochem. Photobiol.*, in press.

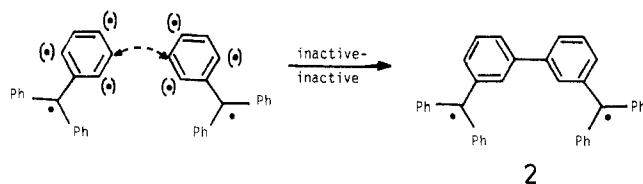
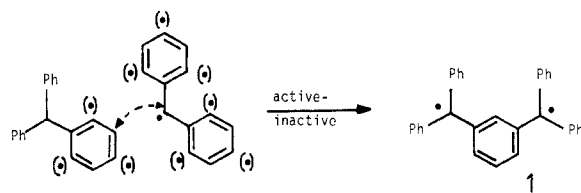
## Synthesis of Two Bis-*m*-quinomethanes. An Experimental Study of Connectivity Effects on the Equal-Parity Criterion for Low-Spin Ground States in Alternant Non-Kekulé Molecules

David E. Seeger,<sup>1a</sup> Paul M. Lahti,<sup>1a</sup> Angelo R. Rossi,<sup>1b</sup> and Jerome A. Berson\*<sup>1a</sup>

Contribution from the Department of Chemistry, Yale University, New Haven, Connecticut 06511, and the Department of Chemistry, University of Connecticut, Storrs, Connecticut 06268. Received August 1, 1985

**Abstract:** As tests of quantum mechanical theories that predict the spin of the ground state of non-Kekulé molecules, precursors to two such species were synthesized: the " $C_{2v}$ " series, initiated by photolysis of 1*H*,1*aH*,2*H*,4*H*,4*aH*,5*H*,5*aH*,6*bH*-1,5-dimethylenedicycloprop[*a,h*]-*s*-indacene-2,4-dione (**13**) to a primary triplet photolysis product, which upon selective further irradiation is converted to 3,6-dimethylenanthracenediyl-1,8-dioxy (**7**), and the " $C_{2h}$ " series, initiated by photolysis of 1*H*,1*aH*,2*H*,3*bH*,4*H*,4*aH*,5*H*,6*bH*-1,4-dimethylenedicycloprop[*a,g*]-*s*-indacene-2,5-dione (**12**), which is converted by a similar two-stage photolysis to 2,6-dimethylenanthracenediyl-4,8-dioxy (**6**). The photoreactions are monitored by EPR and UV-vis spectroscopy. The " $C_{2v}$ " series secondary product (**7**) is a quintet tetraradical in its ground state, whereas the " $C_{2h}$ " series secondary product (**6**) is most probably a triplet biradical in its ground state. In the latter case, the observed adherence to Hund's rule is unexpected, since the substance is an equal-parity alternant system. Connectivity features of **6** that may restore some of the exchange coupling and perturb the inactive-inactive connectivity of an idealized equal-parity case are discussed.

Hückel<sup>2</sup> was the first to point out that making a union<sup>3a</sup> between inactive<sup>3b</sup> sites of two hydrocarbon radicals could lead to a biradical with a low-spin ground state, in violation of Hund's rule.<sup>4</sup> An illustrative case was provided by the pair of hydrocarbons **1** and **2**, synthesized in 1915 by Schlenk and Brauns.<sup>5</sup> Compound **1**



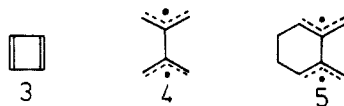
(1) (a) Yale University. (b) University of Connecticut.  
 (2) Hückel, E. *Z. Phys. Chem., Abt. B* **1936**, *34*, 339.  
 (3) (a) See: Dewar, M. J. S. "The Molecular Orbital Theory of Organic Chemistry"; McGraw-Hill: New York, 1969; p 194. (b) An inactive site in an odd alternant hydrocarbon is one at which the NBMO coefficient vanishes (see ref 3a, p 216 and references cited therein).  
 (4) (a) Although Hund's rule originally was promulgated for atoms,<sup>4b</sup> its application to molecules followed soon afterward.<sup>4c-e</sup> The first two applications to organic biradicals were to **1** and **2**.<sup>4f,g</sup> Given the paucity of related experimental data and the primitive state of molecular quantum theory at the time, the immediate recognition<sup>2</sup> that **1** and **2**, although superficially similar in structure, were likely to be fundamentally disparate in magnetic properties can only be regarded as remarkable. (b) Hund, F. "Linienspektren und periodisches System der Elemente"; Springer-Verlag: Berlin, 1927; p 124ff. (c) Hund, F. *Z. Phys.* **1928**, *51*, 759. (d) Mulliken, R. S. *Phys. Rev.* **1928**, *32*, 186. (e) We thank Professor F. Hund for directing our attention to ref 4c and 4d. (f) Hund, F., as cited in ref 4g. (g) Müller, E.; Bunge, W. *Ber.* **1936**, *69*, 2168. (h) For later relevant application of Hund's rule to  $\pi$ -conjugated biradicals, see inter alia: Longuet-Higgins, H. C. *J. Chem. Phys.* **1950**, *18*, 265.

is derived conceptually by an active-inactive union, whereas **2** can be constructed only by an inactive-inactive union. Since the simple HMO  $\pi$ -electron coefficients at inactive sites are zero, the exchange interaction of the two uniting moieties forming **2** is ex-

(5) Schlenk, W.; Brauns, M. *Ber.* **1915**, *48*, 661, 716.

pected to be very small, and hence the difference in energy between the triplet and lowest singlet states of this biradical should be small.<sup>2</sup>

Recently, this basic theme has been strengthened by several elegant and powerful generalizations which teach how to recognize candidate structures that might violate Hund's rule.<sup>6-8</sup> The first two of these<sup>6,7</sup> are probably the easiest for organic chemists to apply. In the Borden-Davidson formalism,<sup>6</sup> if the nonbonding (NB) MO's are (or by linear combinations can be) confined to separate regions of the molecule, they are said to be *disjoint*. This property, to first order, erases the Coulombic repulsion that usually destabilizes the singlet in  $\pi$ -conjugated biradicals. In fact, a higher order effect, dynamic spin polarization, can selectively stabilize the singlet and produce a violation of Hund's rule. Two examples of this have been confirmed computationally at a reasonably high level: square-planar cyclobutadiene<sup>38c-8</sup> and tetramethyleneethane (4),<sup>6</sup> each of which is predicted to have a singlet ground state. It will be noted that 4 is formed by an inactive-inactive union and in fact may be considered the simplest such biradical.



The Ovchinnikov formalism,<sup>7</sup> which is derived from a Heisenberg Hamiltonian within a valence-bond framework, predicts the total electronic spin of the ground state of an alternant system to be given by half the difference between the numbers of starred and unstarred  $\pi$ -centers (eq 1). This predicts singlet ground states

$$S = (n^* - n) / 2 \quad (1)$$

(multiplicity =  $2S + 1$ ) for systems (e.g., 2, 3, 4, and 5) with *equal parity*. It has been shown<sup>6</sup> that such systems are a subset of the disjoint class.

Experimental verifications of these predictions, however, are not available. Thus, cyclobutadiene (3) is not square,<sup>9</sup> and both tetramethyleneethane (TME, 4)<sup>10,11</sup> and the Schlenk-Brauns hydrocarbon 2 probably are nonplanar, so that none of these molecules provides a proper test. The TME derivative 5 presumably is planar or nearly so, but the experimental evidence so far does not seem to permit an unequivocal assignment of the ground state.<sup>12</sup>

The present paper describes a test of eq 1 in the form of the bis-*m*-quinomethanoid biradical 6,<sup>13</sup> which is an equal-parity system and hence should have a singlet ground state. Note that eq 1 is proposed to hold even in heteroatom perturbed  $\pi$ -conjugated systems,<sup>7</sup> an assumption that is supported computationally<sup>14</sup> and experimentally<sup>15,16</sup> in simpler *m*-quinonoid compounds.

(6) Borden, W. T.; Davidson, E. R. *J. Am. Chem. Soc.* **1977**, *99*, 4587. (7) (a) Ovchinnikov, A. A. *Theor. Chim. Acta* **1978**, *47*, 497. (b) Miskurkin, I. A.; Ovchinnikov, A. A. *Russ. Chem. Rev. (Engl. Transl.)* **1977**, *46*, 967.

(8) (a) Klein, D. J. *Pure Appl. Chem.* **1983**, *55*, 299. (b) Klein, D. J.; Nelin, C. J.; Alexander, S.; Matsen, F. A. *J. Chem. Phys.* **1982**, *77*, 3101. (c) Said, M.; Maynau, D.; Malrieu, J.-P.; Garcia Bach, M.-A. *J. Am. Chem. Soc.* **1984**, *106*, 571. (d) Döhnert, D.; Koutecky, J. *J. Am. Chem. Soc.* **1980**, *102*, 1789. (e) Buenker, R. J.; Peyerimhoff, S. D. *J. Chem. Phys.* **1968**, *48*, 354. (f) Kollmar, H.; Staemmler, V. *Theor. Chim. Acta* **1978**, *48*, 223. (g) Borden, W. T.; Davidson, E. R.; Hart, P. J. *J. Am. Chem. Soc.* **1978**, *100*, 388.

(9) (a) Masamune, S.; Souto-Bachiller, F. A.; Machiguchi, T.; Bertie, J. E. *J. Am. Chem. Soc.* **1978**, *100*, 4889. (b) Whitman, D. W.; Carpenter, B. K. *J. Am. Chem. Soc.* **1980**, *102*, 4272.

(10) Dowd, P. *J. Am. Chem. Soc.* **1970**, *92*, 1066.

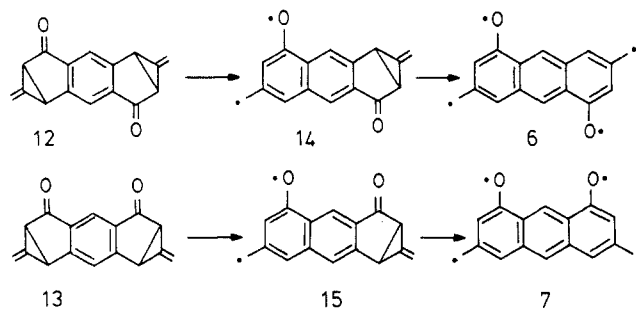
(11) (a) Dixon, D. A.; Foster, R.; Halgren, T.; Lipscomb, W. N. *J. Am. Chem. Soc.* **1978**, *100*, 1359. (b) For a review, see: Gajewski, J. J. "Hydrocarbon Thermal Isomerizations"; Academic Press: New York, 1981; pp 138-155.

(12) (a) Roth, W. R.; Erker, W. *Angew. Chem., Intl. Ed. Engl.* **1973**, *12*, 503. (b) Grimme, W.; Rother, H. *J. Am. Chem. Soc.* **1973**, *95*, 502. (c) Bauld, N. L.; Chang, C.-S. *J. Am. Chem. Soc.* **1972**, *94*, 7594. (d) Roth, W. R.; Scholz, B. P. *Chem. Ber.* **1982**, *115*, 1197.

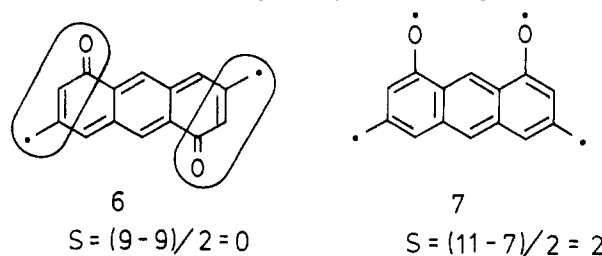
(13) Preliminary communications: Seeger, D. E.; Berson, J. A. *J. Am. Chem. Soc.* **1983**, *105*, 5144, 5146.

(14) Lahti, P. M.; Rossi, A. R.; Berson, J. A. *J. Am. Chem. Soc.* **1985**, *107*, 2273.

### Scheme I

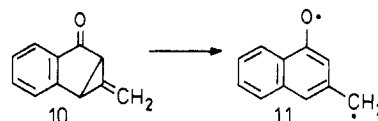
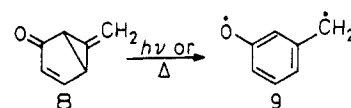


The biradical 6 is related to the simplest disjoint system TME (4) in the sense that the Hückel NBMO electron density is confined to the two (ringed) pentadienyl moieties disjointly. The rigid conjugated framework prevents twisting about the connection between the inactive sites. Moreover, we assumed that the large contribution of aromatic resonance structures would favor the chemical stability of 6 and probably facilitate its generation and



observation. As a "control" experiment, we planned to synthesize the isomeric molecule 7, which is nondisjoint and formally a tetraradical. The qualitative spin rules<sup>4,6,7</sup> predict 7 to be a ground state quintet species.

*m*-Quinomethanes can be generated by thermal or photochemical ring-cleavage of 6-methylenebicyclo[3.1.0]hex-3-en-2-ones, e.g., 8  $\rightarrow$  9<sup>15a,c</sup> and 10  $\rightarrow$  11.<sup>15b,c</sup> By analogy, the logical



precursors for the target molecules 6 and 7 are the isomeric pentacyclic diketones 12 and 13, respectively. Ring-opening of these substances might be expected to occur in two successive stages, via the primary intermediates 14 and 15 (Scheme I).

**Syntheses.** The pentacyclic diketones 12 and 13, precursors to the bis-*m*-quinomethanoids 6 and 7, were prepared by adaptation of the chemistry previously used<sup>15</sup> to synthesize the precursors 8 and 10 related to the mono-*m*-quinomethanoids, 9 and 11. The first stages of the syntheses are outlined in Scheme II, which shows the preparation and characterization of two key intermediate *s*-hydrindacenediones, 17 and 18, from the known<sup>17</sup> *s*-hydrindacen-1-one, 16. Benzylic bromination of 16, hydrolysis of the resulting mixture of bromo ketones to hydroxy ketones, and oxidation with pyridinium chlorochromate<sup>18</sup> gave a mixture from

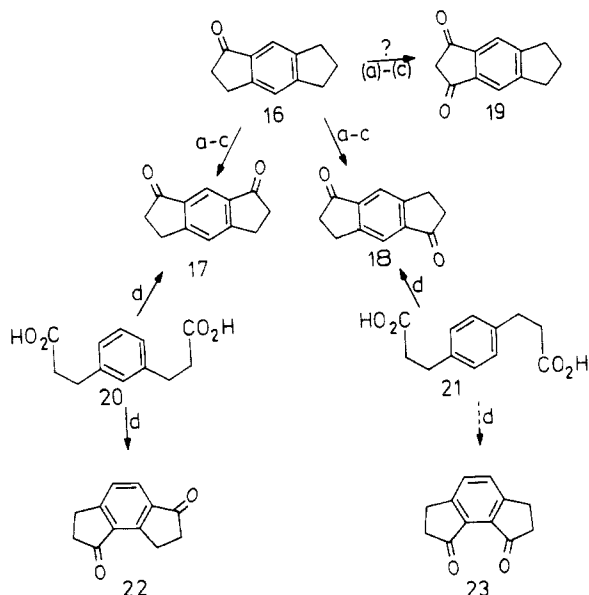
(15) (a) Rule, M.; Matlin, A. R.; Dougherty, D. A.; Hilinski, E. F.; Berson, J. A. *J. Am. Chem. Soc.* **1979**, *101*, 5098. (b) Seeger, D. E.; Hilinski, E. F.; Berson, J. A. *Ibid.* **1981**, *103*, 720. (c) Rule, M.; Matlin, A. R.; Seeger, D. E.; Hilinski, E. F.; Dougherty, D. A.; Berson, J. A. *Tetrahedron* **1982**, *38*, 787. (d) Matlin, A. R.; Inglin, T. A.; Berson, J. A. *J. Am. Chem. Soc.* **1982**, *104*, 4954.

(16) Platz, M. S.; Burns, J. R. *Ibid.* **1979**, *101*, 4425.

(17) Arnold, R. T.; Rondstedt, E. *J. Am. Chem. Soc.* **1945**, *67*, 1265.

(18) Corey, E. J.; Suggs, J. W. *Tetrahedron Lett.* **1975**, 2647.

Scheme II



Methods: (a) NBS,  $\text{CCl}_4$ ; (b) 10%  $\text{H}_2\text{SO}_4$ , THF; (c) PCC,  $\text{CH}_2\text{Cl}_2$ ; (d) PPA.

which *s*-hydrindacene-1,7-dione (**17**) and *s*-hydrindacene-1,5-dione (**18**) could be isolated by high-pressure liquid chromatography in overall yields of 24 and 26%, respectively. A third component was observed in the mixture and may have been *s*-hydrindacene-1,3-dione, **19**, although it was not further identified.

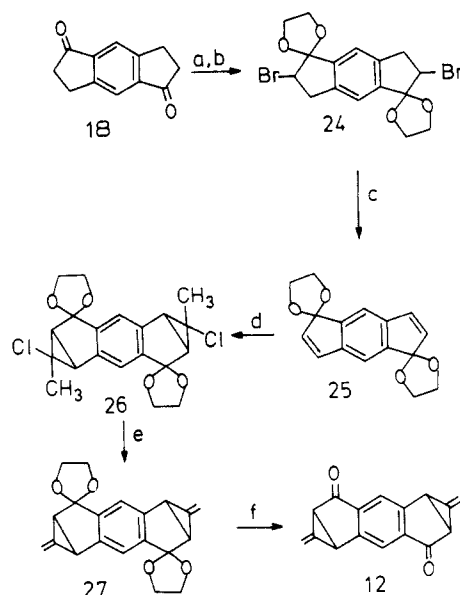
Alternative approaches to **17** and **18** were investigated in an attempt to find a more efficient synthesis (Scheme II). Thus, polyphosphoric acid (PPA) cyclization of *m*-benzenedipropanoic acid, **20**, gave two hydrindacenediones, **17** and (probably) **22**, in very low yields. Compound **17** was identical with one of the diketones obtained from **16**. The formation of **17** by this route, although not preparatively useful, did serve a significant purpose in strengthening the structural assignment, which is crucial to the connectivity analysis. Similarly, PPA cyclization of *p*-benzenedipropanoic acid, **21**, gave a low yield of diketone **18**, identical with the second *s*-hydrindacenedione obtained from **16**. We were unable to detect the *as*-hydrindacenedione, **23**, which might have been expected as a second product from the cyclization of **21**.

The observations of Scheme II leave no doubt about the assignments of  $C_{2h}$  and  $C_{2v}$  symmetries to the two *s*-hydrindacenediones. These molecular point group designations are preserved in the final non-Kekulé molecules **6** and **7**, respectively. The routes to the pentacyclic diketone precursors, **12** and **13**, are shown in Schemes III and IV.

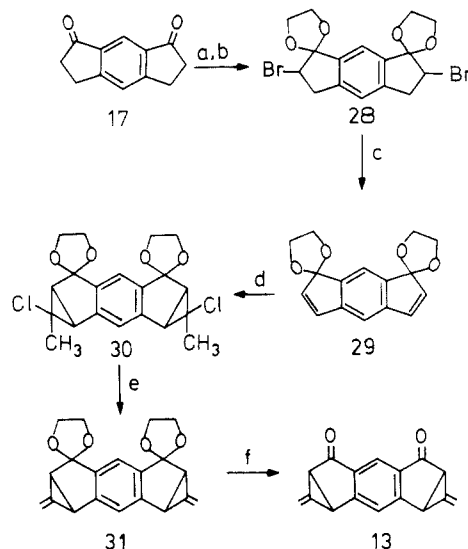
In both sequences, the overall strategy involves protection of the carbonyl groups by ketalization, followed by introduction of two double bonds which serve as receptor sites for a subsequent methylchlorocyclopropanation. Double dehydrohalogenation completes the two methylenecyclopropane units, whereupon the ketal protecting groups in **27** (Scheme III) or **31** (Scheme IV) are removed to give the desired pentacyclic diketone, **12** or **13**, respectively.

Both **12** and **13** are obtained as pairs of stereoisomers which in each case are chromatographically separable and have distinguishable  $^1\text{H}$  and  $^{13}\text{C}$  NMR spectra. The photochemical behavior to be described, however, is not stereospecific.

**Low-Temperature Photolyses. Characterization of Non-Kekulé Species.** The sequential ring-opening events projected in Scheme I can be effected by photolysis and can be tracked by both electron paramagnetic resonance (EPR) and optical (UV-vis) spectroscopy. Photolysis for 30 s with a filtered mercury arc ( $305 \leq \lambda \leq 525$  nm) of a degassed sample of diketone **13** in 2-methyltetrahydrofuran (2-MTHF) at 36 K in the cavity of the EPR spectrometer results in the generation of an orange-red color and the appearance of a primary EPR signal, the  $\Delta m_s = \pm 1$  region of

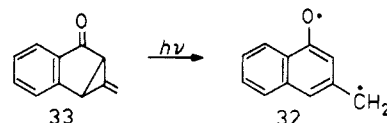
 Scheme III. ( $C_{2h}$  Series")


Methods: (a)  $\text{Br}_2$ , HOAc; (b)  $\text{HOCH}_2\text{CH}_2\text{OH}$ , TsOH, PhH; (c) KOH, MeOH; (d)  $\text{CH}_3\text{CHCl}_2$ , BuLi, reflux; (e) KOtBu,  $\text{Me}_2\text{SO}$ ; (f) 10%  $\text{H}_2\text{SO}_4$ , THF.

 Scheme IV. ( $C_{2v}$  Series")


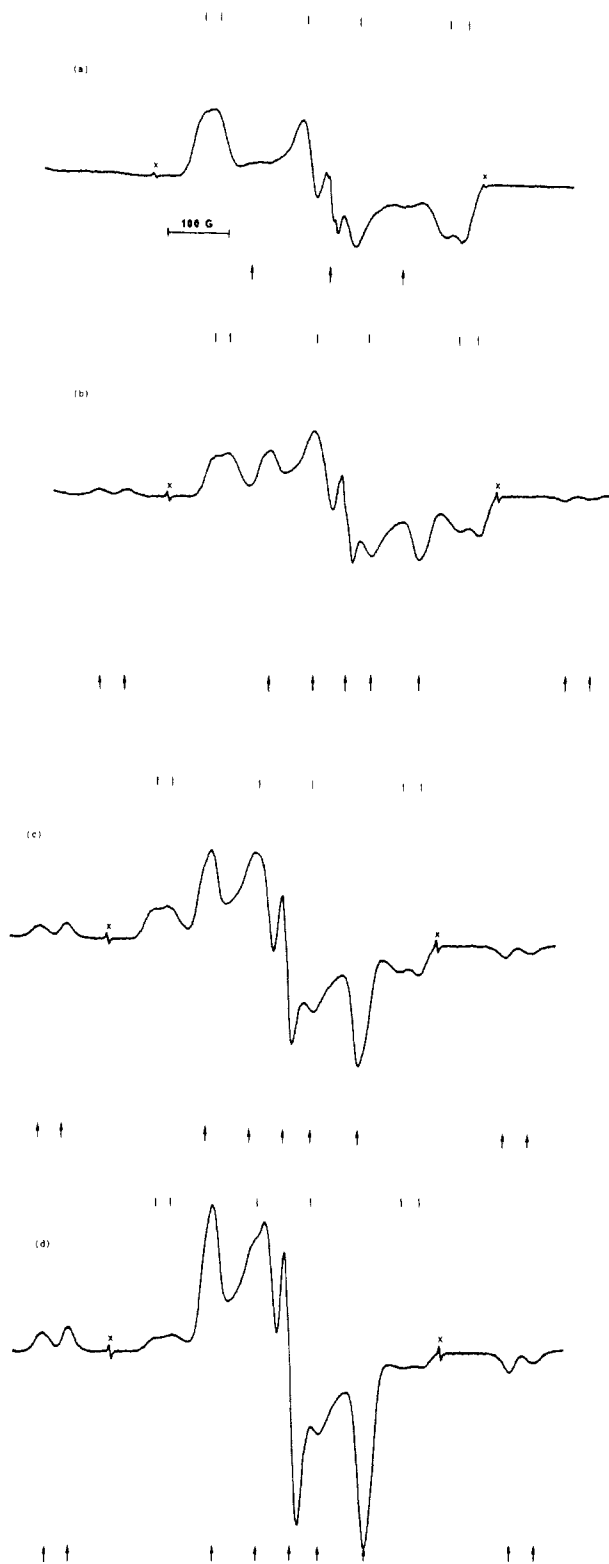
Methods: same as in Scheme III.

which is centered near 3260 G and is shown in Figure 1a. The EPR spectrum is typical of a randomly oriented triplet species<sup>19</sup> with the zero-field splitting (ZFS) parameters  $|D|/hc \approx 0.020$  and  $|E|/hc \approx 0.005 \text{ cm}^{-1}$ . Also, a weak resonance (not shown) corresponding to the two-quantum ( $\Delta m_s = \pm 2$ ) transition can be seen at approximately half the magnetic field ( $\sim 1620\text{G}$ ) and is diagnostic of a triplet paramagnetic species. The ZFS parameters are in good agreement with those ( $|D|/hc = 0.0204$ ,  $|E|/hc = 0.0052 \text{ cm}^{-1}$ ) of the model triplet biradical **32** previously ob-



served<sup>15b,c</sup> in the photolysis of the ketone **33**. The parallel methods of synthesis and closely corresponding EPR spectra justify the

(19) Wasserman, E.; Hutton, R. S. *Acc. Chem. Res.* 1977, 10, 27 and references cited therein.



**Figure 1.** EPR spectra from photolysis of diketone **13** in 2-MTHF glass at 36 K. The lines and arrows mark the positions of transitions associated with the triplet state of biradical **15** and the quintet state of tetradical **7**, respectively. The symbol X marks absorption by H atoms. All the spectra were recorded with the same spectrometer control settings. (a) After 30 s irradiation at  $305 \text{ nm} \leq \lambda \leq 525 \text{ nm}$ . (b) After 10 min at  $\lambda > 425 \text{ nm}$ . (c) After 35 min at  $\lambda > 425 \text{ nm}$ . (d) After 180 min at  $\lambda > 425 \text{ nm}$ .

identification of the carrier of the spectrum of Figure 1a as the triplet state of the substituted *m*-naphthoquinomethane **15** (see Scheme I).

A close examination of Figure 1a shows faint indications that, even after only 30 s of photolysis, a second paramagnetic species

is being generated. The resonances associated with this product are marked with arrows and can be observed to grow slowly stronger at the expense of the main spectrum by prolonged irradiation at  $305 \text{ nm} \leq \lambda \leq 525 \text{ nm}$ . This observation suggested that the new species was a product of secondary photolysis of the biradical **15**. Under the stated wavelength photolysis conditions, it would be difficult to drive the secondary photolysis to completion because the short wavelength region of the mercury arc emission (principally 313 and 366 nm) passed by the filter would be strongly absorbed by the diketone starting material **12** ( $\lambda_{\lambda_{\text{max}}}$  338, 278, 270, 232 nm), photolysis of which would replenish the primary product **15**. However, it was possible to force the second photon into **15** by taking advantage of the long-wavelength absorption associated with its orange color (see below). Irradiation of a preparation of the primary product **15** at  $\lambda > 425 \text{ nm}$  resulted in the gradual disappearance of the primary EPR spectrum and its replacement by a new spectrum (Figure 1). At the same time, the orange color of **15** changed to red-purple (see below). We assign the EPR spectrum of the secondary photoproduct to a quintet state of the tetradical **7**.

The secondary spectrum is wider, more complex, and more intense than the primary one. It consists of at least nine discernible widely spaced lines which span a range of nearly 800 G. The signal persists in the dark at 36 K, and its shape is independent of temperature over the range 15–80 K. That the secondary spectrum does not result merely from a photoreaction of the primary triplet **15** with the matrix was implied by a control experiment which showed that irradiation of the model triplet **32** at  $\lambda > 425 \text{ nm}$  at 77 K in 2-MTHF did not change the EPR spectrum.

The most fully developed secondary EPR spectrum we have been able to obtain (Figure 1c) is from a sample that still contained some unconverted triplet primary product **15**, which can be detected by the persistence of weak bands at the positions marked by lines. After 180 min of irradiation, the reaction was incomplete and was proceeding only slowly, presumably because of the internal filter effect of the accumulating intensely colored secondary species, whose optical absorption overlaps that of the primary product **15** (see below). Perhaps a more complete conversion could be achieved by the use of a monochromator or a laser with an emission wavelength that would be absorbed only by biradical **15**, but the optical spectra (see below) do not offer much encouragement that this will be easy.

Nevertheless, the conversion of triplet **15** to a species of higher spin (**7**) is clear from the growth in intensity during the photolysis at  $\lambda > 425 \text{ nm}$ . This increase cannot be attributed to photolysis of the diketone **13** (which is essentially transparent at these wavelengths) and, therefore, must represent a net increase in the total number of spins during the reaction which generates the secondary signal carrier. If this triplet  $\rightarrow$  quintet reaction were quantitative, the signal intensity should increase by a factor of 2.0, were it not for the statistical factor (see Appendix A) which causes transitions between adjacent quintet state sublevels to be inherently  $6/5$  as probable as the corresponding ones of the triplet. Since the total number of free electron spins doubles in the triplet  $\rightarrow$  quintet conversion, the signal intensity should increase by a factor of  $12/5$  or 2.4. The experimental difficulties already described have prevented a quantitative test of this prediction, but we have been able to push the secondary photoreaction to the point where the doubly integrated spectral intensity of the (mostly) secondary product is 1.7 times that of the primary one.

Although the increase in signal intensity is probably the most compelling and direct evidence for a triplet  $\rightarrow$  quintet conversion, an analysis of the details of the spectrum provides useful corroboration.

Since the EPR spectroscopy<sup>20</sup> of quintet species is likely to be unfamiliar to the general reader, we provide in the main text the principal features of the theory, together with an outline of the

(20) For general references, see: (a) Wertz, J. E.; Bolton, J. R. "Electron Spin Resonance: Elementary Theory and Practical Applications"; McGraw Hill: New York, 1967. (b) Weltner, W., Jr. "Magnetic Atoms and Molecules"; Scientific and Academic Editions: New York, 1983.

**Table I.** Fit of the Observed Line Positions of the Quintet Tetradical **15** to a Quintet Hamiltonian

resonance field, G		direction (H//x, y, or z)	error, % <sup>b</sup>
obsd	calcd <sup>a</sup>		
2893	2894	z	0.1
2931	2930	y	0.1
3151 <sup>c</sup>	3142	z	1.2
3151 <sup>c</sup>	3152	y	0.1
3232	3234	x	0.3
3265 <sup>c</sup>	3248	x	2.3
3265 <sup>c</sup>	3272	x	0.9
3315	3308	x	0.9
3380 <sup>c</sup>	3378	y	0.3
3380 <sup>c</sup>	3392	z	1.6
3609	3608	y	0.1
3645	3646	z	0.1

<sup>a</sup>For the turning points of the spectrum, microwave frequency 9.175 GHz,  $D = 0.01174 \text{ cm}^{-1}$ ,  $E = 0.00315 \text{ cm}^{-1}$ ,  $g = 2.0054$ . <sup>b</sup>% of the total spectral width. <sup>c</sup>It is assumed that two transitions are coincident at this position.

procedures we used to fit the observed spectrum to a quintet Hamiltonian and to extract the zero-field splitting parameters. Details are given in Appendix B.

For each canonical orientation of a quintet molecule, four nearest-neighbor ( $\Delta m_s = \pm 1$ ) "allowed" EPR transitions are expected. Since all three orientations are represented in a powder or glassy dispersion, as many as twelve transitions might be observed. In some cases, coincidences of positions for different transitions reduce the total number of distinguishable lines. The "forbidden" absorptions ( $\Delta m_s = \pm 2, 3, 4$ ) in principle are possible but may be difficult to observe with X-band instruments because the resonance condition requires fields high enough to fully field-quantize the energy levels and enforce the nearest-neighbor selection rule. In a few instances,<sup>21</sup> the multiple-quantum quintet transitions have been observed at low magnetic fields.

To demonstrate that the observed spectrum can be fitted to a quintet Hamiltonian, one can begin by estimating the values of  $D'$  and  $E'$ , the zero-field splitting (ZFS) parameters (in field units, G) by inspection of the spectrum, using the perturbationally derived<sup>22</sup> approximate solutions (eq 2 and 3) of the Hamiltonian

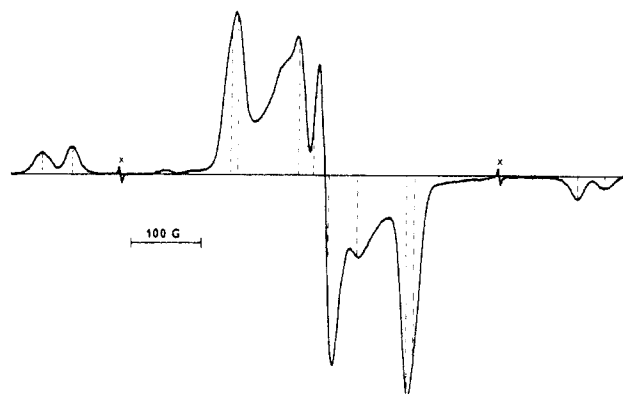
$$H_1 = H_0 + 3D' \quad (2)$$

$$H_2 = H_0 + \frac{3}{2}(D' + 3E') \quad (3)$$

$$H = g\beta H_x S_x + g\beta H_y S_y + g\beta H_z S_z + D[S_z^2 - \frac{1}{3}S^2] + E[S_x^2 - S_y^2] \quad (4)$$

matrix (eq 4). Note that eq 4 is an approximation in that it takes into account only the Zeeman (first three terms) and spin-dipolar (last two terms) interactions and does not treat spin-orbit and higher order terms. This approximation is unlikely to cause difficulty with ZFS as small as that observed here but may need to be refined with larger ZFS.<sup>23</sup> In eq 2 and 3,  $H_0$  is the field at the center of the spectrum, whereas  $H_1$  and  $H_2$  represent the positions of the two highest field transitions.

The Hamiltonian of eq 4 can be used to determine the energy level diagram and the positions (and intensities) of absorption by substitution of the spin matrices appropriate to the basis functions of the quintet state:  $|+2\rangle$ ,  $|+1\rangle$ ,  $|0\rangle$ ,  $|-1\rangle$ , and  $|-2\rangle$ . The spin matrices can be constructed by using known<sup>24</sup> equations to evaluate the nonvanishing matrix elements. Diagonalization of the matrix



**Figure 2.** Derivative-mode EPR spectrum of the quintet tetradical **7** after subtraction from Figure 1d of the spectral contribution of residual triplet **15**. The dashed lines show the calculated positions for the 12 transitions (Table I). Note that whereas the turning points of the outer lines correspond to steps in absorption mode and, hence, appear as maxima (or minima), the central line corresponds to an absorption maximum and hence appears as a derivative feature with two extrema.

yields the eigenvalues and eigenvectors. The positions of the  $\Delta m_s = \pm 1$  transitions are found by finding the points at which the energy gaps between the nearest-neighbor pairs of sublevels,  $|+2\rangle \leftrightarrow |+1\rangle$ ,  $|+1\rangle \leftrightarrow |0\rangle$ ,  $|0\rangle \leftrightarrow |-1\rangle$ , and  $|-1\rangle \leftrightarrow |-2\rangle$ , are equal to the microwave energy. The transition probabilities are the squares of the off-diagonal matrix elements connecting the two sublevels,  $(\langle Q|\hat{S}_i|Q'\rangle)^2$ , where  $\langle Q|$  and  $|Q'\rangle$  are the sublevels involved in the transition.

We have used the values of  $D'$  and  $E'$  estimated from eq 2 and 3 as starting input data for matching the positions of the observed transitions. Varying  $D'$ ,  $E'$ , and  $g$  (the electronic  $g$ -factor) to obtain a satisfactory simulation was achieved by the procedure and computer program described in Appendix B. No attempt was made to match the intensities. Table I shows the best fit we were able to achieve. After multiplications of  $D'$  and  $E'$  by  $g\beta$  to convert to the unit basis, the "best" values were  $|D|/hc = 0.01174 \text{ cm}^{-1}$ ,  $|E|/hc = 0.00315 \text{ cm}^{-1}$ , and  $g = 2.0054$ . Figure 2 displays the quintet spectrum of **7**, obtained by subtraction of the background due to residual **15**, and shows graphically the match of the calculated and observed line positions. The spectrum shows only nine of the theoretically possible twelve resonances, which suggests the occurrence of three close coincidences of lines. It is significant that the simulation not only provides appropriate field positions for the observed transitions but also predicts the three coincidences (Table I). We emphasize that the successful simulation uses disposable parameters and, hence, does not guarantee a unique solution. However, although the fit provides permissive rather than decisive evidence of structure, it nevertheless is a comforting adjunct to the intensity measurements already described.<sup>25,26</sup> Further corroboration might come from a low-field detection of the multiple quantum transitions ( $\Delta m_s = \pm 2, 3, 4$ ) with an L-band

(25) That the spectrum of **7** can be simulated with the approximate spin matrix of eq 4 suggests that the contribution of higher order terms (see ref 23) to the ZFS is small in this case. Similarly, the quintet matrix derived from eq 4 neglects mixing of the quintet sublevels of appropriate symmetry with nearby singlet states, which in some instances (see ref 27) can shift the ZF levels and hence the relative positions of the EPR transitions from those of the "pure" quintet state by as much as 5–10%. The successful simulation in the case of **7** (maximum deviation 2.3%) suggests that the assumption of a pure quintet state for the carrier of the spectrum is valid.

(26) Although the value of the ZFS parameter  $D$ , in the spin-dipolar approximation, is inversely related to the average separation of the electrons and hence contains structural information, the comparison of  $D$ -values for species of two different multiplicities is not readily interpretable. This can be seen from the equation<sup>28</sup>

$$D = \left(\frac{3}{4}\right)g^2\beta^2F \sum \left\langle \frac{1}{r^3} - \frac{3z}{r^5} \right\rangle$$

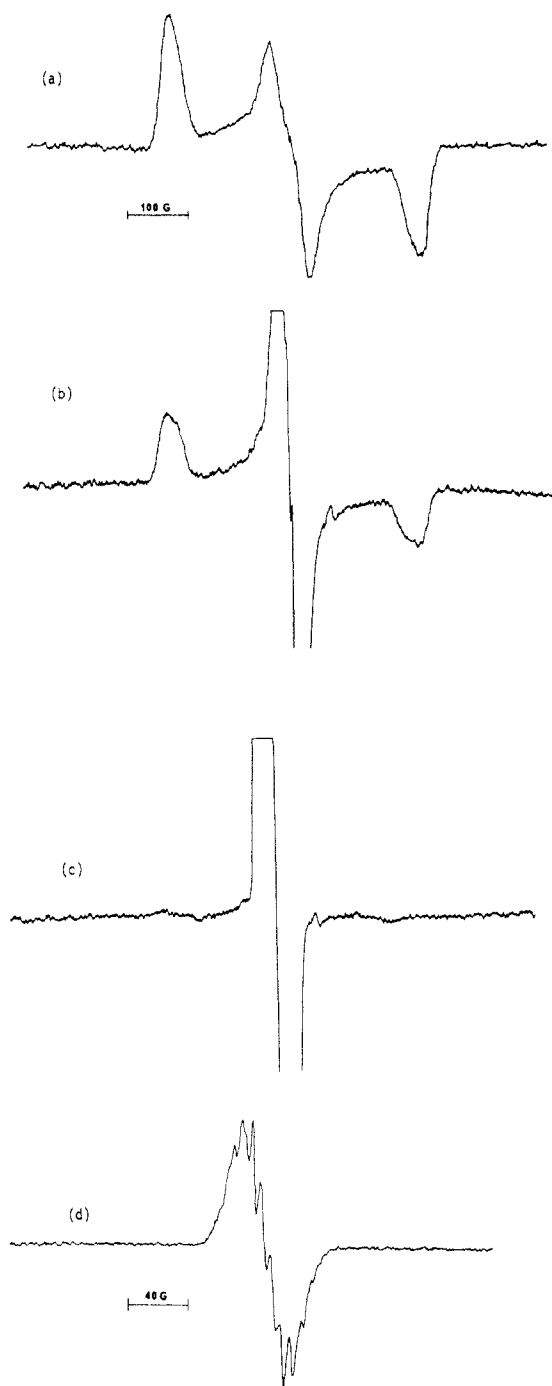
where the distance-sensitive bracketed expectation value signifies an average over the electronic wavefunction, and  $F = 2!(2S-2)!/(2S)!$ . Since  $0! = 1$  by definition, the factor  $F$  has the values 1 and  $1/6$  for triplet and quintet species, respectively.

(21) (a) Huber, R.; Schwoerer, M. *Chem. Phys. Lett.* **1980**, *72*, 10. (b) Schwoerer, M.; Huber, R. A.; Hartl, W. *Chem. Phys.* **1981**, *55*, 97.

(22) Wasserman, E.; Murray, R. W.; Yager, W. A.; Trozzolo, A. M.; Smolinsky, G. *J. Am. Chem. Soc.* **1967**, *89*, 5076.

(23) For discussions of more accurate Hamiltonians for systems with  $S > 1$ , see: (a) Abragam, A.; Bleaney, B. "Electron Paramagnetic Resonance of Transition Ions"; Oxford University Press: Oxford, England, 1970. (b) Huber, R. Ph.D. Thesis, Universität Bayreuth, 1981, as cited in ref 21.

(24) (a) Reference 20a, Appendix B, especially pp 427–434. (b) See also: Dowsing, R. D. *J. Magn. Reson.* **1970**, *2*, 332.

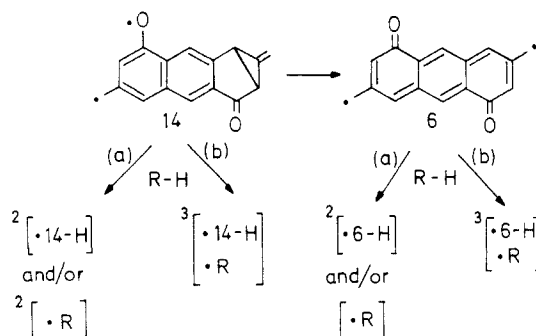


**Figure 3.** EPR spectra obtained from photolysis of diketone **12** in 2-MTHF glass at 77 K. Spectra a-c were recorded with the same spectrometer settings. Spectrum d is of the same preparation as c, except that the x-axis has been expanded and the y-axis contracted. (a) After 30 s,  $305 \leq \lambda \leq 525$  nm. The spectral contribution of a small amount of secondary photoproduct has been digitally subtracted. (b) After an addition 4 min of photolysis,  $\lambda \geq 425$  nm. (c) After 81 min,  $\lambda \geq 425$  nm. (d) Same preparation as c with altered scale.

EPR spectrometer. These transitions so far have eluded observation by the X-band instrument available to us.

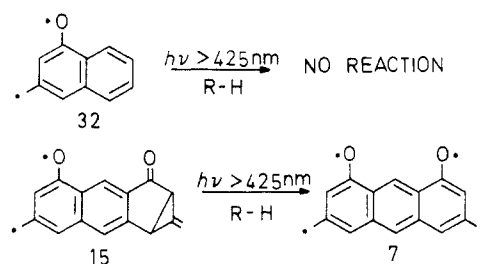
**EPR Characterization of Non-Kekulé Species in the Sequence  $12 \rightarrow 14 \rightarrow 6$  (Scheme I).** Irradiation (30 s,  $305 \leq \lambda \leq 525$  nm) of a sample of the diketone **12**, the precursor of the  $C_{2h}$  biradical **6**, in 2-MTHF glass at 77 K in the EPR spectrometer cavity again gave rise to a red-orange color (see below) and a spectrum of a randomly oriented triplet species (Figure 3a). In this case,  $|D|/hc \sim 0.020$   $\text{cm}^{-1}$ , and  $|E|/hc \sim 0.007$   $\text{cm}^{-1}$ . The  $|D|/hc$  value is approximately the same as those of the other two naphthoquinodimethanes **32** and **15** and justifies the assignment of the carrier of the triplet spectrum as the primary photoproduct **14**,

**Scheme V.** Hypothetical Photoreactions of **14** Giving EPR-Active Products upon Irradiation at 425 nm



(a) Hydrogen abstraction from solvent forming two isolated doublet monoradicals. (b) Hydrogen abstraction from solvent forming a triplet radical pair.

**Scheme VI**



with one of the two bridge bonds of **12** having been broken. The triplet nature of the primary signal carrier is confirmed by the observation of the weak  $\Delta m_s = \pm 2$  transition near 1630 G.

As we had done in the " $C_{2v}$ " series (**13**  $\rightarrow$  **15**  $\rightarrow$  **7**), we took advantage of the long-wavelength absorption of **14** to force the second photon into the triplet species of the " $C_{2h}$ " series **12**  $\rightarrow$  **14**  $\rightarrow$  **6**. Irradiation of the frozen preparation of **14** at  $\lambda \geq 425$  nm caused the primary EPR signal and orange color of **14** to fade and be replaced by a new signal (Figure 3) and a red-purple color. After prolonged irradiation, the primary triplet signal associated with **14** had almost completely disappeared and a new, extremely intense narrow band had grown up in the middle of the spectrum. When brought on scale instrumentally, this secondary spectrum was revealed to consist of a narrow cluster of lines, with the positive and negative maxima separated by only  $\sim 40$  G.

Control experiments showed that no EPR spectrum was produced upon irradiation of frozen, degassed 2-MTHF through either of the filters ( $305 < \lambda < 525$  nm or  $\lambda > 425$  nm) or upon irradiation of a frozen, degassed solution of the diketone **12** at  $\lambda > 425$  nm.

That the carrier of the secondary EPR spectrum of Figure 3 is a triplet species is not immediately evident, because the compellingly diagnostic "forbidden"  $\Delta m_s = \pm 2$  transition at half-field could not be observed. However, since the ZFS is very small ( $|D|/hc \approx 0.0025$   $\text{cm}^{-1}$ ), this transition is expected to be strongly forbidden (see above), so that its absence does not rule out a triplet signal carrier.

Scheme V outlines several hypothetical reactions that could give rise to EPR active species from the primary photoproduct **14**. We now put forward experiments and arguments that exclude all of these but the triplet state of the  $C_{2h}$  biradical **6** as the secondary photoproduct whose spectrum is shown in Figure 3d.

One class of photoproducts that might be imagined includes those derived from the primary biradical **14** by photoinduced hydrogen abstraction from the glassy medium. This could give rise to a pair of doublet radicals,  $\cdot 14\text{-H}$  and  $\cdot \text{R}$ , or to a matrix-caged triplet pair of these radicals (Scheme V). The reaction seems inherently unlikely since, as has already been reported, the model triplet biradical **32** undergoes no photoreaction at all in  $>425$ -nm light, and the even more closely related triplet **15** does not abstract

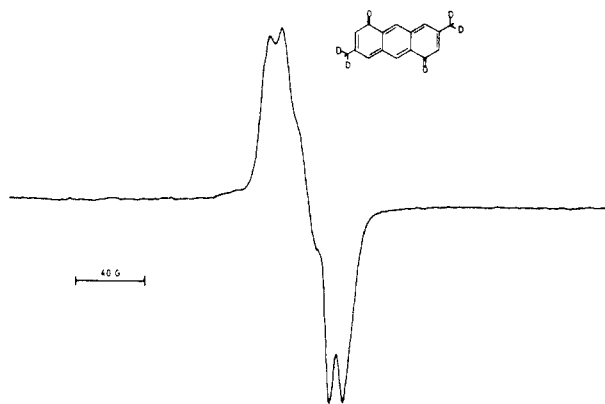


Figure 4. Secondary EPR spectrum obtained (similarly to that of Figure 3d) from the photolysis of **12-d<sub>4</sub>**. The triplet ZFS parameters are  $|D|/hc = 0.0025 \text{ cm}^{-1}$  and  $|E|/hc = 0.0009 \text{ cm}^{-1}$ .

hydrogen but instead undergoes cleavage of its remaining methylenecyclopropane ring to give **7** (Scheme VI). Moreover, the spectrum of the two doublets or the triplet derived when **14** abstracts hydrogen should depend on the solvent, but we observed the same spectra in ethanol and ethanol-*d*<sub>6</sub> glasses as those obtained in 2-MTHF. The only way to account for a medium-independent EPR spectrum by the hydrogen abstraction pathway is to assume that the solvent radical  $\cdot R$  reacts (by unspecified means) to give an EPR inactive product, leaving only the doublet radical  $\cdot 14-H$ . If the reaction were quantitative, as Figure 3 suggests,  $14 \rightarrow \cdot 14-H$  would result in a net decrease of 50% in the total number of spins and a decrease of the EPR signal intensity to  $3/8$  of the value observed for **14** (see Appendix A). A similar argument applies to the hypothetical pathway  $6 \rightarrow \cdot 6-H$  (Scheme V).

To test this prediction, we prepared a sample of primary biradical **14** by a brief (10 s) irradiation of diketone **12** in order to avoid over-irradiation and concomitant generation of secondary product. After carefully digitizing and double integrating this spectrum (see Experimental Section for details), we irradiated the sample through the long-wavelength-passing filter ( $\lambda > 425 \text{ nm}$ ) until the primary spectrum had been completely replaced by the secondary one. Digitization and integration gave an intensity value within the experimental error ( $\sim 8\%$ ) of that of the primary spectrum. Although the error limits are too broad to permit a confident distinction between a triplet  $\rightarrow$  triplet reaction and a triplet  $\rightarrow$  two doublets reaction, they clearly rule out a triplet  $\rightarrow$  one doublet process. Combined with the medium-independence of the spectra, this result suffices to exclude all but the triplet  $14 \rightarrow$  triplet **6** conversion in Scheme V.

At least eight lines are observed in the EPR spectrum of the secondary triplet (Figure 3d), which is more than the number that could be produced merely from the spin-dipolar interaction in a triplet state. None of the lines is attributable to a two-photon transition (absorption of two microwave quanta), which normally appears as a sharp line in the middle of the spectrum.<sup>20</sup> The intensity of such a transition should decrease relative to the normal (one-photon) spectrum as the microwave power is decreased, but we find that decreasing the power weakens all the lines uniformly and does not change the shape of the spectrum.

By substitution of deuterium for protium at appropriate sites, we were able to show that the complexity of the secondary spectrum of Figure 3d is the result of proton hyperfine coupling. Theoretically, the disjoint nature of the biradical **6** would predict that the exocyclic methylene groups would carry most of the carbon-centered spin density in **6**, which would cause the hyperfine coupling of the protons at those sites to be the largest in the molecule. A repetition of the synthesis of Scheme III with  $\text{CD}_3\text{CHCl}_2$  instead of  $\text{CH}_3\text{CHCl}_2$  gave the diketone **12-d<sub>4</sub>**. Irradiation in the usual two-stage manner of a degassed glassy 2-MTHF sample of **12-d<sub>4</sub>** gave a primary EPR spectrum which is not significantly different from that of the primary spectrum of undeuterated **12**, but the secondary spectrum is vastly simplified

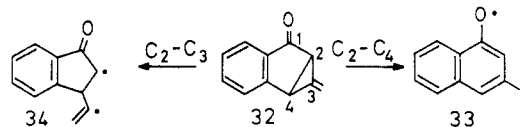
Table II. Experimental Refutations of Candidate Structures for the Carrier of the Secondary EPR Signal in the Photolysis of **14**<sup>a</sup>

candidate structure <sup>b</sup>	experiment		
	solvc	label <sup>d</sup>	intensity <sup>e</sup>
$^2[\cdot 14-H] + ^2[\cdot R]$	X	X	X (?)
$^3[\cdot 14-H-R]$	X	X	-
$^2[\cdot 14-H]$	-	-	X
$^3[\cdot 6]$	-	-	-

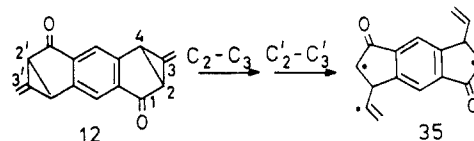
<sup>a</sup> A matrix element  $X_{ij}$  indicates refutation of structure *i* by experiment *j*. A dash (-) element indicates that the candidate cannot be eliminated by the corresponding experiment. <sup>b</sup> See Scheme V. <sup>c</sup> Change of solvent. <sup>d</sup> Isotopic labeling in **12-d<sub>4</sub>**. <sup>e</sup> Comparison of doubly integrated intensities of primary and secondary spectra.

(Figure 4). In fact, aside from some small residual hyperfine splitting which seems to be present near the center, the spectrum of Figure 4 is consistent with that of a randomly oriented triplet species in which  $|D| \approx 3|E|$ . The triplet ZF parameters  $|D|/hc \approx 0.0025 \text{ cm}^{-1}$  and  $|E|/hc \approx 0.0009 \text{ cm}^{-1}$  may be extracted.

The small value of  $|D|$  is consistent with the weak spin-dipolar interaction expected of biradical **6**, in which the disjoint character of the NBMO's tends to confine the unpaired electrons to widely separated spatial domains at the outer edges of the molecule. Moreover, the small splitting observed provides a welcome additional piece of structural information on the course of the photolytic reactions of the triketoones **12** and **13** (Scheme I) and the benzenone **32**. A referee of a previous paper<sup>15c</sup> has made



the point that the EPR spectrum we assigned as naphthoquinomethane **33** might instead be caused by a triplet species **34**, arising from cleavage of the "wrong" bond ( $\text{C}_2-\text{C}_3$ ) of **32**, instead of the bridge bond  $\text{C}_2-\text{C}_4$ . The finding of a total spectral width of only  $\sim 40 \text{ G}$  for the secondary signal (Figure 3) in the photolysis of the analogous ketone **12** supplements previous arguments<sup>15c</sup> against



"wrong-bond" cleavage: the resulting hypothetical species **35** would be a vinyl radical, whose hyperfine splitting alone would be larger than the observed total width.<sup>29</sup>

The simplification of the EPR spectrum of the secondary product from **12-d<sub>4</sub>** (compare Figures 3d and 4) strongly confirms the previous inferences that the carrier of the spectrum must be derived at least in part from the precursor diketone. Combined with the above observations that the secondary spectrum is not changed by the use of different glassy media, these data make it difficult to ascribe any part of the spectrum to another source.

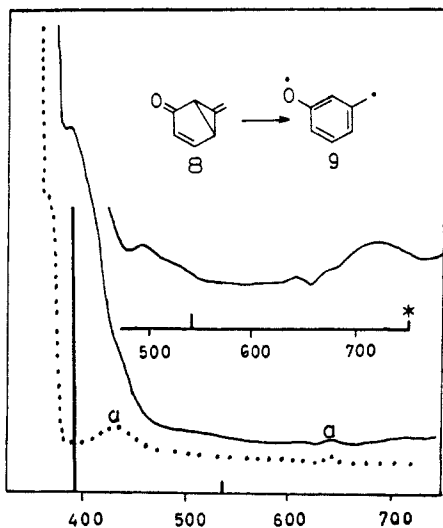
Table II is a refutation matrix which summarizes these tests of the compatibility of the candidates of Scheme V with the experimental facts. The only candidate to survive this scrutiny is the triplet biradical **6**. The EPR evidence, thus, is in accord with the two sequential reactions projected in Scheme I, when the spin states are specified as singlet  $12 \rightarrow$  triplet  $14 \rightarrow$  triplet **6** and singlet  $13 \rightarrow$  triplet  $15 \rightarrow$  quintet **7**. Optical spectroscopic evidence for both sequential ring-openings will be described now.

Experimental and Theoretical UV-vis Absorption Spectroscopy of the Photolytically Generated Non-Kekulé Species. As already

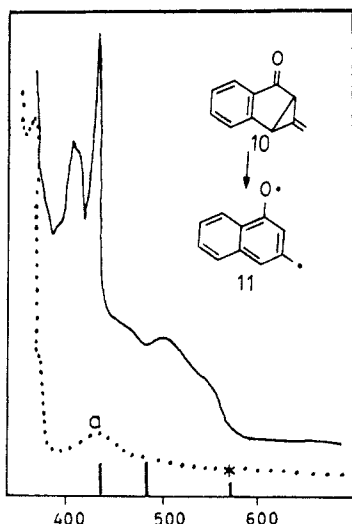
(27) Benk, H.; Sixl, H. *Mol. Phys.* **1981**, *42*, 779.

(28) (a) Higuchi, J. *J. Chem. Phys.* **1963**, *38*, 1237. (b) Higuchi, J. **1964**, *39*, 1847.

(29) (a) Fessenden, R. W.; Schuler, R. H. *J. Chem. Phys.* **1963**, *39*, 2147. (b) Reference 20a, p 214.



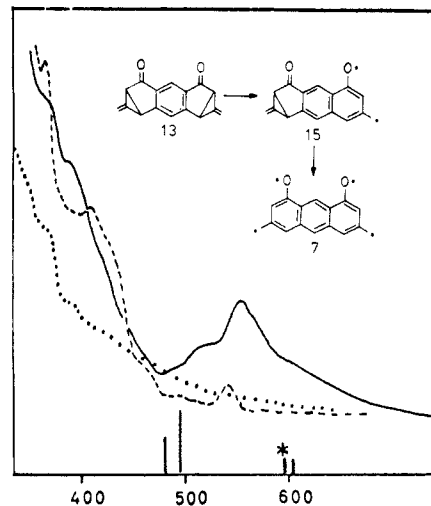
**Figure 5.** Optical spectra of preparations of *m*-quinomethane **9** triplet state in EtOH glass at 15 K obtained by irradiation of ketone **8**. The vertical bars mark the locations and relative intensities calculated by INDO/S-CI theory. The asterisk (\*) marks the predicted location of the longest wavelength  $n,\pi^*$  band:  $\cdots$ , before irradiation;  $-$ , after irradiation at 220–440 nm for 1 m. The features marked "a" are base line artefacts.



**Figure 6.** Same as caption for Figure 5 but for *m*-naphthoquinomethane **11**.

has been mentioned, the photochemical generation of the non-Kekulé species of Scheme I and of the closely related analogues **9** and **11** is accompanied by spectacular visual color phenomena. Figures 5 and 6 show the spectra<sup>30</sup> responsible for the yellow and orange colors, respectively, generated when the bicyclic and tricyclic ketones **8** and **10** are photolyzed by using the  $220 < \lambda < 440$  nm filter with a mercury arc lamp at 15 K in EtOH glasses. Under these conditions, the irradiating wavelength is nominally 313-nm light. We assign these spectra to the triplet-triplet transitions of *m*-quinomethane **9** and *m*-naphthoquinomethane **11**. The wavelengths and relative intensities calculated by INDO/S-CI (see Theoretical Section) for the optical transitions are indicated by the vertical bars. Although the two strong, short-wavelength bands of **11** (Figure 6) are bathochromically shifted in isopentane–Et<sub>2</sub>O ( $\lambda_{\max}$  452, 428 nm) relative to those in EtOH ( $\lambda_{\max}$  437, 404 nm), the long-wavelength band is hardly changed ( $\lambda_{\max}$  504 vs. 500 nm). This insensitivity plays a diagnostic role in a later context.

(30) Since the precursor ketones of the non-Kekulé species always remain in large excess, and since at the experimental concentrations their absorption envelopes extend into the near UV, it is difficult to measure the non-Kekulé transitions below  $\sim 380$  nm.



**Figure 7.** Optical spectra at 16 K in EtOH glass obtained by irradiation of the diketone **13** successively at 220–440 nm to give the triplet **15** and then at  $>425$  nm to give the quintet **7**:  $\cdots$ , before irradiation;  $- - -$ , primary photolysis product **15**;  $-$ , secondary product **7**. Transitions shown by vertical bars are calculated for **7**.

The visual bathochromic shift associated with benzannulation (**9** yellow vs. **11** orange) prompts the hypothesis that the extra conjugation in **11** decreases the  $\pi,\pi^*$  transition energy. However, this idea is not born out by the calculations, which suggest a more complicated reason. The longest wavelength  $\pi,\pi^*$  transition is predicted to occur at 540 nm for **9** and at 485 nm for the more highly conjugated **8**, the reverse order from that of the oversimplified picture. However, the 540-nm band of **9** is predicted to be very weak, with an oscillator strength ( $f$ ) of  $5 \times 10^{-4}$ , only a sixtieth of that predicted for the 485-nm band of **11**. The visible spectrum of **9**, therefore, is dominated by a strong band that appears at 420 nm (predicted 393 nm) as a shoulder on the tail of the absorption of the ketone **8**.

The low-energy  $n,\pi^*$  band of *m*-naphthoquinomethane **11** is predicted to occur near 573 nm (Figure 6, asterisk) with  $f = 3 \times 10^{-4}$  and is presumably hidden under the  $\pi,\pi^*$  envelope. The corresponding transition for *m*-quinomethane **9** is predicted (Figure 1, asterisk) at 753 nm with  $f \leq 10^{-4}$  and probably accounts for the broad band which is just discernible near 710 nm at higher spectrum amplitude.

The INDO/S-CI calculation is semiempirical, and there is a dearth of known examples of non-Kekulé molecules upon which to test it.<sup>31</sup> Therefore, correspondences of predicted and observed spectroscopic features cannot be taken as diagnostic. Nevertheless, the generally close agreements seen in Figures 5–8 suggest at least that the transitions have been correctly identified.

Below 70 K, the optical spectra of **9** and **11** are stable for at least 5 h after irradiation is ended. In each case, the spectra remain unchanged up to about 100 K, above which temperature the bands disappear simultaneously, leaving the spectrum of the remaining unphotolyzed ketone precursor.

Further confirmatory information on the carrier of the UV-vis spectrum of *m*-naphthoquinomethane **11**, the product observed upon photolysis of glasses of ketone **10**, is now available from a study<sup>32</sup> of the picosecond flash photolysis in fluid media. Two successive transients can be observed: A, a singlet with a solvent-dependent UV-vis spectrum and lifetime ( $\tau \sim 750$  ps in benzene), and B, a triplet, long-lived on the picosecond time scale, with a UV-vis spectrum nearly solvent-independent ( $\lambda_{\max}$  500–505 nm in cyclohexane, benzene, or CH<sub>3</sub>CN). The position and insensitivity to solvent observed for the long-wavelength absorption

(31) For calculations of optical transitions of non-Kekulé species by PP-P-CI methods see: (a) Muller, J.-F.; Muller, D.; Dewey, H. J.; Michl, J. *J. Am. Chem. Soc.* **1978**, *100*, 1629. (b) Gisin, M.; Rommel, E.; Wirz, J.; Burnett, M. N.; Pagni, R. M. *Ibid.* **1979**, *101*, 2216. (c) Gisin, M.; Wirz, J. *Helv. Chim. Acta* **1983**, *66*, 1556.

(32) Goodman, J. L.; Peters, K. S.; Lahti, P. M.; Berson, J. A. *J. Am. Chem. Soc.* **1985**, *107*, 276.

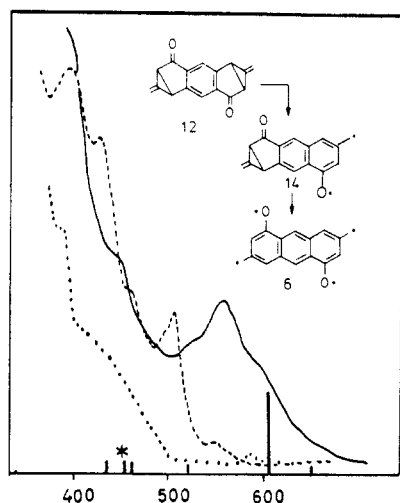


Figure 8. Similar to Figure 7 for the process 12 (···) → 14 (---) → 6 (—). Transitions shown by vertical bars are calculated for 6.

maximum of the orange paramagnetic preparation obtained from ketone 10,  $\lambda_{\text{max}}$  500 nm (EtOH), 504 nm (5:1 isopentane-Et<sub>2</sub>O), match those of transient B and support the assignment of a triplet species 11 as the common carrier of the UV-vis spectrum in fluid medium and of the UV-vis and EPR spectra in glasses.

Figure 7 shows the sequence of events in the photolysis of the precursor ketone 13 of the C<sub>2v</sub> series. Brief irradiation using nominal 13-nm conditions produced a visible orange color and an optical spectrum with maxima at 544 nm (weak) and 416 nm (strong) and a shoulder near 440 nm. These primary absorptions are similar to those of *m*-naphthoquinomethane 11 (Figure 6) and suggest that the initial photolysis has opened one ring of the C<sub>2v</sub> precursor ketone (13 → 15). When the irradiating light was switched to  $\lambda > 425$  nm, the visible color soon changed to red-purple, and the primary spectrum faded to be replaced by a new one. The secondary spectrum shows a shoulder near 520 nm and a broad maximum near 560 nm which slopes deeply into the visible region beyond 600 nm. We assign the secondary spectrum to the quintet biradical 7 by analogy to the corresponding set of sequential changes previously observed in the EPR-monitored photolysis.

The positions and relative intensities calculated for the quintet-quintet absorption of 7 are shown (Figure 7). Since no model compounds have been available to parameterize the INDO/S-CI calculation for Q-Q transitions, the present calculations for 7 used triplet parameters. As Figure 7 shows, the results are in reasonable accord with the observed absorptions, but the agreement could be fortuitous, and caution is urged in applying this expedient to other systems.

A similar set of sequential spectroscopic changes can be observed (Figure 8) in the photolysis of the C<sub>2h</sub> precursor diketone 12: first an orange color is formed, resulting from a primary spectrum of triplet 14, with maxima at 540 (weak), 495, 430, and 420 nm. This is superseded, after further photolysis at  $>425$  nm, by a secondary spectrum,  $\lambda_{\text{max}}$  560, shoulders 530, 600 nm, associated with the red-purple visible color of triplet 6. Again, the INDO/S-CI calculation gives fairly good agreement with the observed secondary spectrum (Figure 8).

The UV-vis spectroscopic studies support the EPR observations in demonstrating sequential events in the photolyses of the C<sub>2v</sub> and C<sub>2h</sub> precursor diketones. Moreover, the insensitivity of the spectra of Figure 7 and 8 to temperatures in the range 15–70 K is consistent with the EPR evidence against thermal population of more than one spin state.

**Spin of the Ground State of the C<sub>2v</sub> Molecule 7.** The shape of the EPR spectrum of the quintet species 7 does not change with temperature, but the signal intensity (*I*) follows the Curie-Weiss law (eq 5), where *C* and  $\theta$  are constants, between 15 and 70 K.

$$I = \frac{C}{T - \theta} \quad (5)$$

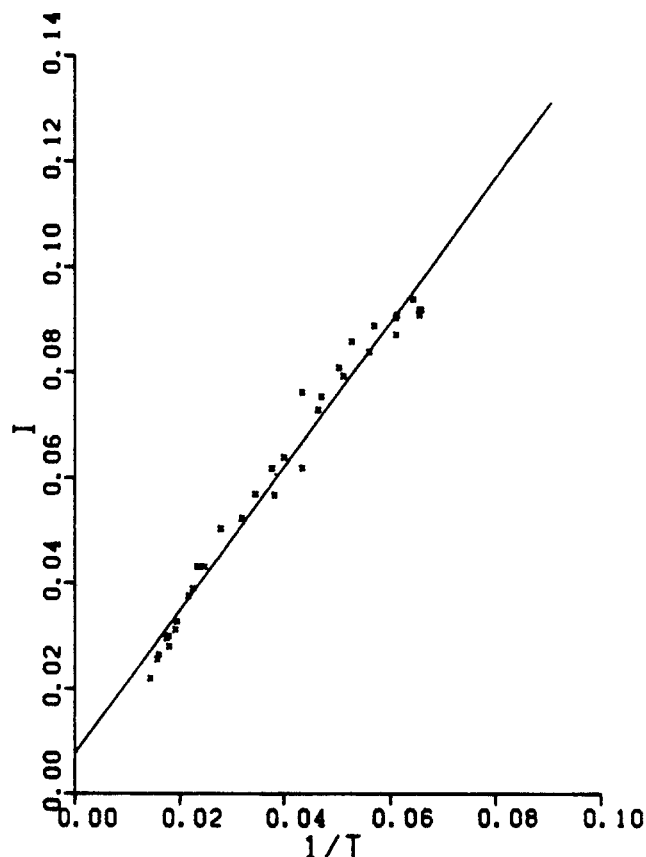


Figure 9. Curie-Weiss least-squares analysis ( $r = 0.988$ ) of EPR signal intensity as a function of reciprocal absolute temperature for the quintet species 7. The glassy medium is 2-MTHF, the temperature range is 15–70 K, and the microwave power is 0.01 mW.

Table III. Pairs of Energy States

	case								
	1	2	3	4	5	6	7 <sup>a</sup>	8 <sup>a</sup>	9 <sup>a</sup>
order of	S	Q	T	Q	T	S	Q, S	Q, T	T, S
states <sup>b</sup>	Q	S	Q	T	S	T			

<sup>a</sup>Degenerate pair. <sup>b</sup>The energies of the states decrease from upper to lower.

For the plot of *I* vs. reciprocal absolute temperature (Figure 9), data were collected by successive measurements in both increasing and decreasing temperature directions. The absence of any hysteresis effect indicates that the temperature-induced change is reversible. The correlation coefficient, 0.988, is not as good as that seen with the C<sub>2h</sub> species 6 (see below), and the convex direction of deviation from linearity at lower temperatures suggests that saturation of the transitions is not negligible. This was confirmed by a saturation plot (*I* vs.  $P^{1/2}$ , where *P* is the microwave power) at 15.7 K, which clearly deviates from linearity even at low microwave powers ( $P \sim 0.1$  mW). The question remains whether saturation effects account for all of the deviation or whether part of the downward curvature at low temperatures is caused by depopulation of the quintet state to one or more species of neighboring energy. A "worst case" estimate of the energy separation of the quintet state from such hypothetical species can be made on the (demonstrably false) assumption that all of the curvature in the Curie plot is attributable to this depletion of the quintet. The problem is complicated by the fact that two neighboring additional states, a triplet and/or a singlet, might be populated. From the three states, singlet (S), triplet (T), and quintet (Q), nine pairs and thirteen triads can be constructed by permutation of the energy orderings. It is convenient to consider the pairs first (Table III).

For reasons already given, a major contributor to the EPR spectrum must be a quintet, which immediately eliminates cases

Table IV. Triads of Energy States

	case					
	10	11	12	13	14	15
order of states <sup>b</sup>	Q	Q	T	T	S	S
	T	S	Q	S	T	Q
	S	T	S	Q	Q	T

	case						
	16	17	18	19	20	21	22
order of states <sup>b</sup>	Q	T, S <sup>a</sup>	T	Q, S <sup>a</sup>	S	Q, T <sup>a</sup>	Q, T, S <sup>a</sup>
	T, S <sup>a</sup>	Q	Q, S <sup>a</sup>	T	Q, T <sup>a</sup>	S	

<sup>a</sup>Degenerate group. <sup>b</sup>The energies of the states decrease from upper to lower.

5, 6, and 9. Of the remaining choices, only cases 2 and 4 involve excited quintet states.

In case 2, the Curie–Weiss data can be fitted to a curved form by assuming that the singlet and quintet are in equilibrium over the temperature range of the measurements and that the singlet is the ground state by a few small calories. From the difference in energy,  $\Delta E = E_Q - E_S$ , between the quintet and hypothetical singlet states, the Boltzmann relationship, and the multiplicity factor, the equilibrium constant may be derived as in eq 6. The

$$\frac{[\text{quintet}]_{\text{eq}}}{[\text{singlet}]_{\text{eq}}} = 5e^{-\Delta E/RT} \quad (6)$$

observation that the Curie behavior is reversible justifies the assumption that no chemical reaction other than interconversion of spin states occurs over the temperature range of the Curie plot. Therefore, the sum of the concentrations of the quintet and singlet species is constant. Since the signal intensity is proportional to the total number of quintet molecules in the sample, eq 5 and 6 may be manipulated to give eq 7.

$$I = \frac{C}{T - \theta} \left[ \frac{5e^{-\Delta E/RT}}{1 + 5e^{-\Delta E/RT}} \right] \quad (7)$$

To fit the experimental data to eq 7, we estimate initial values for the Curie–Weiss constants  $C$  and  $\theta$  from the linear portion of the plot. These are then used with trial values of  $\Delta E$  until the best fit to the experimental data is found. The procedure is crude and no doubt would be improved by more sophisticated algorithmic techniques, but the accuracy of the data does not justify such refinement. A value for  $\Delta E$  of about 0.036 kcal/mol is found to give a fit to the data that is no worse than the least-squares line of Figure 9. Since some of the curvature is known to be caused by saturation, this value is an upper limit. We may conclude, therefore, that case 2 does not apply but has become case 7, where the quintet and singlet are exactly degenerate or nearly so. This seems inherently improbable, especially since case 7 ascribes no role to the triplet, the state of intermediate multiplicity.

In case 4, both the quintet and triplet contribute to the signal intensity, but the inherent probability of a quintet transition is 2.4 times that of a triplet (see Appendix A). Thus, the total intensity may be expressed as in eq 8, which assumes that the

$$I = \frac{2.4C_q}{T - \theta_q} \left[ \frac{5e^{-\Delta E/RT}}{3 + 5e^{-\Delta E/RT}} \right] + \frac{C_t}{T - \theta_t} \left[ \frac{3e^{-\Delta E/RT}}{3 + 5e^{-\Delta E/RT}} \right] \quad (8)$$

quintet and triplet species independently follow eq 5. On the reasonable assumption that the Curie–Weiss constants of the two species do not differ much, a curve-fitting procedure similar to that described for case 2 may be applied to the experimental data by using eq 8, from which it is deduced that the triplet might be as much as 0.027 kcal/mol below the quintet. However, this value for  $\Delta E$  would require that the [quintet]/[triplet] concentration ratio change from 0.67 at 15 K to 1.43 at 90 K. This switch in the dominant populations would be manifest in changes in the EPR and UV–vis spectra, but these are not observed. Case 4 is, therefore, eliminated.

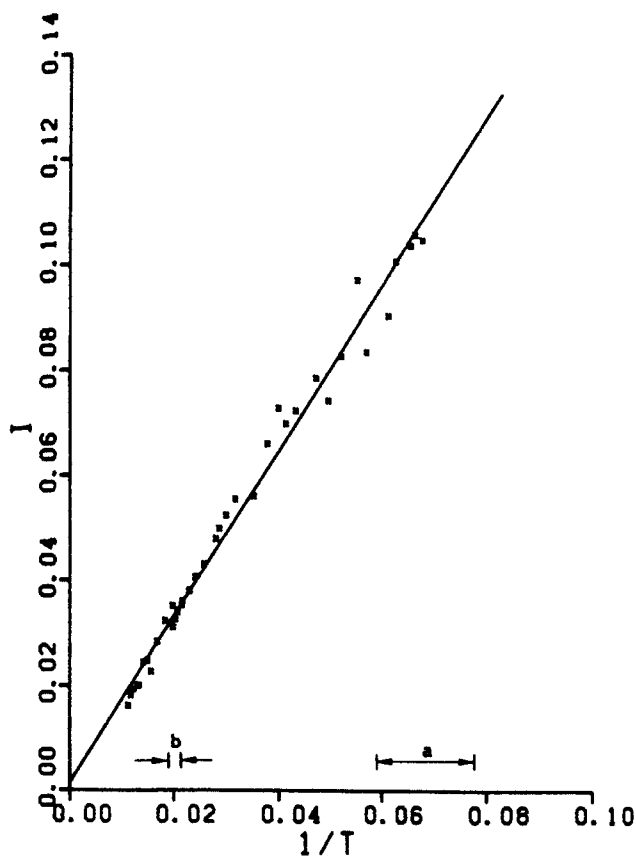


Figure 10. Curie–Weiss least-squares analysis ( $r = 0.991$ ) of EPR signal intensity as a function of reciprocal absolute temperature for the triplet species 6. The glassy medium is 2-MTHF, the temperature range is 15–90 K, and microwave power is 0.01 mW. The error bars marked “a” and “b” represent  $15 \pm 2$  and  $50 \pm 2$  K, respectively.

The remaining alternative is case 8, in which the two states Q and T are degenerate ( $\Delta E < 0.005$  kcal/mol), and, hence, the relative populations and spectral line shapes are temperature-independent.

A similar analysis may be applied to the 13 triads (Table IV). Given that the shape of the signal does not change with temperature, the EPR-active states (T and Q) must be degenerate or nearly so, which eliminates cases 10–19. Of the remaining possibilities, only case 21 involves an excited quintet state. The multiplicity factor in the intensity equation now becomes eight, since if  $\Delta E$  were zero, the EPR-active levels Q and T would contain  $8/9$  of the population (eq 9). Fitting the Curie data to eq 8, we

$$I = \frac{C}{T - \theta} \left[ \frac{8e^{-\Delta E/RT}}{1 + 8e^{-\Delta E/RT}} \right] \quad (9)$$

obtain 0.042 kcal/mol for  $\Delta E$ . This near-degeneracy excludes case 21 and leaves case 22, in which all three states are degenerate, a hypothesis that seems even less likely than the twofold degeneracy of case 7. Therefore, the most reasonable ground-state assignment to the  $C_{2v}$  molecule 7 is a quintet.

**Spin of the Ground State of the  $C_{2h}$  Molecule 6.** The temperature dependence of the EPR signal intensity of the triplet species 6 follows the Curie–Weiss law with a correlation coefficient of 0.991 (Figure 10). Again, a saturation plot shows curvature even at low microwave power, so that some curvature is to be expected in the Curie plot. A perhaps more significant source of error is the difficulty of measuring low temperatures accurately for a Curie plot, which is exacerbated by the reciprocal form (see Figure 10). If these and other errors are considered negligible and if a curved Curie plot is attributed entirely to population of the singlet state, the data may be fitted to eq 10<sup>33</sup> with  $E_T - E_S$

$$I = \frac{C}{T - \theta} \left[ \frac{3e^{-\Delta E'/RT}}{1 + 3e^{-\Delta E'/RT}} \right] \quad (10)$$

$= \Delta E' \sim 0.024$  kcal/mol. Realistically, this is an upper limit, since some saturation occurs, so that if the singlet is in equilibrium with the triplet, the two spin states must be almost exactly degenerate. Although this interpretation cannot yet be ruled out rigorously, it rests upon a hypothetical major coincidence and seems a slender basis upon which to claim to have substantiated theory. An alternative and, in our view, more probable interpretation is that the triplet is the ground state by a large enough margin to preclude detectable population of the singlet.

### Discussion

Despite theoretical indications that low-spin ground states in disjoint  $\pi$ -conjugated systems are to be expected, we are not aware that a single such case has been found experimentally.<sup>34</sup> Moreover, the test molecule **6** now seems to contradict the theory, since unless an unlikely exact degeneracy occurs here, the ground state is triplet. However, these experiences are not necessarily to be interpreted as arising from a failure of theory. At least part of the problem so far may be attributable to the difficulty of assigning the ground state when a stable EPR signal cannot be obtained, as seems to be the case in the simple tetramethylethane (TME) systems **4** and **5**.<sup>10,11</sup>

It might be argued that the triplet  $C_{2h}$  species **6** we observe is not the planar molecule needed for a proper test of disjoint character but instead has one or both of the exocyclic methylene groups twisted out of the plane. Although we have no direct evidence on the point, analogy to computational results for other conjugated *triplet* biradicals<sup>11a,35a-d</sup> would suggest that the twisted species would be substantially higher in energy than the planar one. Note that the possibility that methylene twisting may stabilize the *singlet* state of the biradical would only serve to strengthen the present discrepancy, since in that case the planar singlet would be even further above the triplet.

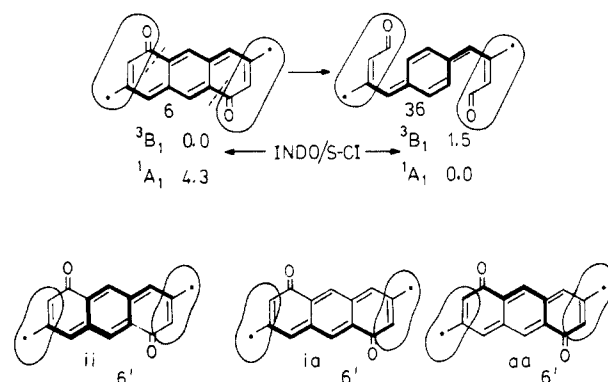
Another objection to **6** as a test molecule might be that the observed triplet is an  $n, \pi^*$  species, rather than the  $\pi, \pi^*$  biradical that is needed for comparison with the corresponding singlet. However, INDO/S-CI calculations<sup>14</sup> give no support to this idea and find the  $n, \pi^*$  states for both **6** and **7** to be substantially higher in energy ( $>29.3$  and  $>27.5$  kcal/mol, respectively) than their all- $\pi$  counterparts.

The apparent breakdown of the qualitative theories in the case of **6** makes it clear that other factors can sometimes override disjoint character. In this connection, we are heartened by the outcome of a calibrated semiempirical calculation,<sup>14</sup> which places the triplet of **6** 4.3 kcal/mol *lower* in energy than the singlet, in qualitative agreement with the experimental observations. Although at this stage these theoretical results cannot be said to have elucidated the underlying physical reasons for the unexpected adherence of this particular disjoint system to Hund's rule, they give us some confidence that INDO/S-CI calculations may provide hints on which non-Kekulé molecules would constitute useful tests of spin-state order and spacing.

Our continuing pursuit of these questions is based upon the assumption that the main idea of the qualitative theories<sup>2,6-8</sup> is correct, namely that the exchange interaction of the SOMO electrons in equal-parity (therefore, disjoint)  $\pi$ -conjugated non-Kekulé molecules is small and, hence, that a singlet should be the ground state or a very low-lying excited state. The problem at present is to perceive the structural features of formally disjoint test molecules that act to restore some of the exchange coupling and thereby contaminate the desired pure test situation.

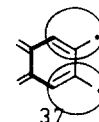
In the case of the biradical **6**, some hint of such contamination has emerged as a result of a calculation<sup>14</sup> we carried out following a suggestion of Professor W. T. Borden. Disconnection of the  $C_1-C_{11}$  and  $C_5-C_{14}$  bonds of the anthracene system of **6** produces

### Scheme VII



the disjoint hypothetical molecule **36** (Scheme VII). This inverts the energy order calculated by INDO/S-CI and restores the singlet ground state. At this level of calculation, the effect is substantial: a change in relative energies of the singlet and triplet of 5.8 kcal/mol. Note that in compound **36**, the (ringed) pentadienyl moieties are joined (heavy lines) only at one inactive position each, whereas in **6**, they are joined at *both* inactive positions. Formally, it is as if the ringed *allyl* moieties in **6'** (Scheme VII) have not only inactive-inactive (ii) but also inactive-active (ia) and active-active (aa) connections. Perhaps these quasiactive connections perturb the pure TME-like connectivity which forms the real basis of the disjoint model.

At present, it would be premature to assume that such connections always will overcome disjoint character. For example, the unknown disjoint molecule 1,2,4,5-tetramethylenebenzene, **37**,



is predicted to have a singlet ground state by both *ab initio*<sup>35e,f</sup> and INDO/S-CI<sup>14</sup> calculations, despite a quasiactive connection of the two formal allyl units. Experimental and theoretical studies of further examples of disjoint systems are needed to systematize these interactions.

### Experimental Section

**Instruments.** Routine nuclear magnetic resonance (NMR) spectra were taken on a Varian EM-360A NMR spectrometer (60 MHz), a Varian EM-390 NMR spectrometer (90 MHz), a Perkin-Elmer R-32 NMR spectrometer (90 MHz), or a JEOL FX-90Q NMR spectrometer (90 MHz) in deuteriochloroform unless otherwise noted. Chemical shifts were measured relative to tetramethylsilane ( $Me_4Si$ ) and reported as follows: chemical shifts (parts per million downfield from  $Me_4Si$ ), multiplicity, number of protons, coupling constant (when measured), and assignment.  $^{13}C$  NMR spectra were recorded on a JEOL FX-90Q in deuteriochloroform unless stated otherwise.

Infrared (IR) spectra were taken on a Beckman 4250 IR spectrophotometer or a Nicolet 7199 FT-IR spectrometer. All absorptions are reported in  $cm^{-1}$  followed by the relative intensity.

Ultraviolet-visible (UV-vis) spectra were obtained on a Cary 219 spectrophotometer.

Mass spectra (MS) were taken on a Hewlett-Packard Model 5985 gas chromatograph/mass spectrometer (GC/MS) system. Most of the spectra were performed by Daniel Pentek whom we thank. High resolution parent molecular ion analyses were performed by Dr. Timothy Wachs of Cornell University.

(33) Breslow, R.; Chang, H. W.; Hill, R.; Wasserman, E. *J. Am. Chem. Soc.* **1967**, *89*, 1112.

(34) (a) Singlet ground states for some nonconjugated biradicals have been demonstrated.<sup>34b,c</sup> In these cases, however, the small magnitude of the exchange coupling is due to relatively efficient insulation of the two spins, not to disjoint character of SOMO  $\pi$ -orbitals. (b) Closs, G. L.; Doubleday, C. *J. Am. Chem. Soc.* **1972**, *94*, 9248; (c) **1973**, *95*, 2735.

(35) (a) Kato, S.; Morokuma, K.; Feller, D.; Davidson, E. R.; Borden, W. T. *J. Am. Chem. Soc.* **1983**, *105*, 1791. (b) Borden, W. T. "Diradicals", Academic Press: New York, 1982; Chapter 1 and references cited therein. (c) Dixon, D. A.; Dunning, T. H., Jr.; Eades, R. A.; Kleier, D. A. *J. Am. Chem. Soc.* **1981**, *103*, 2878. (d) Lahti, P. M., Ph.D. Thesis, Yale University, 1985, Appendix A. (e) Lahti, P. M.; Rossi, A. R.; Berson, J. A. *J. Am. Chem. Soc.* **1985**, *107*, 4362. (f) Du, P.; Hrovat, D.; Borden, W. T.; Lahti, P. M.; Rossi, A. R.; Berson, J. A., submitted for publication.

Elemental analysis was carried out by Dr. R. Rittner of the Olin Corp., New Haven, CT.

Preparative vapor-phase chromatography (VPC) was carried out on a Varian Aerograph Model 920 with helium as the carrier gas in the column specified.

EPR spectra were taken on a Varian E-9 EPR spectrometer. For experiments performed above the boiling point of liquid nitrogen a Varian Model V-4540 variable-temperature accessory was used. An Air Products Model LTD-3-110 liquid transfer heli-tran refrigerator with an Air Products Model APD-E temperature controller was used for experiments below 77 K. The nominal sample temperature was monitored by using a gold (0.07% iron) chromel thermocouple with a thermocouple located a few centimeters below the sample. Samples were irradiated in the cavity of the EPR spectrometer with an Oriol Model 6137 mercury arc lamp.

Spectra that were collected digitally were taken on an LSI 11/23 computer by using a program written by Ronald Merrill. All other programs were written in FORTRAN for Digital Equipment's 11/750 VAX computer.

**Reagents.** All chemicals used synthetically were reagent grade or better. The solvents used for low-temperature EPR studies were purified as follows. 2-Methyltetrahydrofuran was heated at reflux over potassium permanganate overnight and distilled. It was then heated at reflux over lithium aluminum hydride overnight and distilled. This solvent was stored over molecular sieves under nitrogen. Absolute ethanol was stored over molecular sieves.

**Syntheses. 1,7- and 1,5-*s*-Hydrindacenediones (17 and 18) from *s*-Hydrindacen-1-one (16) (Scheme II).** *s*-Hydrindacen-1-one<sup>17</sup> (5 g, 29.1 mmol) was placed in a 500-mL, round-bottomed flask and dissolved in 200 mL of CCl<sub>4</sub>. *N*-Bromosuccinimide (5.23 g, 29.1 mmol) and a few crystals of benzoyl peroxide were then added, and the mixture was brought to reflux. The reaction was complete when the solid was floating. After completion of the reaction, the cooled mixture was filtered, and most of the solvent was removed in vacuo to yield an oily red substance: NMR  $\delta$  7.2–7.8 (m, Ar), 5.4–5.7 (m, geminal to Br), 2.5–3.3 (m).

This crude material was not isolated or characterized but instead was immediately taken up in 100 mL of tetrahydrofuran. To this solution was added 100 mL of 5% H<sub>2</sub>SO<sub>4</sub>, and the reaction was allowed to run overnight. This mixture was then extracted with several portions of ether, and the organic layer was washed with water and brine. The resulting red solution was dried over MgSO<sub>4</sub>, and the solvent was removed in vacuo to yield a dark red oil. The oil was not purified, and progress of the reaction was demonstrated by the new multiplet in the NMR at  $\delta$  5.1–5.4 (H geminal to hydroxyl).

This oil was immediately dissolved in CH<sub>2</sub>Cl<sub>2</sub> (30 mL) and was introduced into a 500-mL, round-bottomed flask charged with pyridinium chlorochromate<sup>18</sup> (9.4 g, 43.6 mmol) in 70 mL of CH<sub>2</sub>Cl<sub>2</sub>. This resulted in a black solution which was stirred for 3 h. Five volumes (500 mL) of ether were used to dilute the reaction mixture, and the liquid was decanted from a black tarry substance, yielding an orange liquid. The remaining black tar was rinsed with a small portion of ether. The combined organic layers were concentrated to ~100 mL at which time crystallization ensued. The crystals were filtered off and were easily purified by column chromatography on silica gel by using a CH<sub>2</sub>Cl<sub>2</sub>/EtOAc (8:1) solvent system. The fractions obtained from this separation contained the isomeric diketones 17 and 18 and some recovered starting material.

The solvent from the remaining ether layer was removed in vacuo, yielding some additional crude product. Separation of this mixture proved to be more difficult due to the presence of an unknown impurity. This impurity has an *r<sub>f</sub>* on silica gel which is intermediate with respect to the *r<sub>f</sub>* values of 17 and 18. Analytical thin-layer chromatography on silica gel with CH<sub>2</sub>Cl<sub>2</sub>/EtOAc (8:1) showed the following: *r<sub>f</sub>* = 0.36 (18), *r<sub>f</sub>* = 0.30 (unknown), and *r<sub>f</sub>* = 0.25 (17). Separation was accomplished by using high-pressure liquid-phase chromatography on a Waters Prep LC/System 500A. The column used was silica gel, and the solvent system was CH<sub>2</sub>Cl<sub>2</sub>/EtOAc (25:1). Confirmation of structure was based on comparison (NMR spectra, melting point, and mixture melting point) with those of independently prepared samples of each diketone. The total overall yields from *s*-hydrindacen-1-one were 0.8 g of 18 (23.6% based on recovered starting material) and 0.9 g of 17 (26.6% based on recovered starting material).

***s*-Hydrindacene-1,7-dione (17).** A sample of 1 g (4.5 mmol) of *m*-benzenedipropanoic acid<sup>36</sup> was added to 30 g of polyphosphoric acid heated to 120 °C in a 100-mL, round-bottomed flask which was fitted with a mechanical stirrer. Heating was continued for 40 min, and then the dark red solution was slowly poured into 300 mL of H<sub>2</sub>O. The aqueous solution was extracted five times with portions of Et<sub>2</sub>O. The

extracts were combined, the solvent was removed in vacuo, and the solid was taken up in THF. To this solution was added a saturated solution of NaHCO<sub>3</sub> to remove the majority of the acidic material. Extracting the fluid with Et<sub>2</sub>O, washing the organic layer with water, drying the Et<sub>2</sub>O layer with MgSO<sub>4</sub>, and removing the solvent resulted in a yellow crystalline material. Separation was achieved by column chromatography on silica gel with petroleum ether/EtOAc (1:4). After chromatography, two isomeric diketones were obtained. The desired diketone 17, which was the second product from the column, was obtained as a white crystalline solid in 3.9% yield (33 mg) after recrystallization from EtOH: NMR  $\delta$  8.05 (s, 1 H, Ar), 7.56 (s, 1 H, Ar), 3.1–3.3 (m, 4 H), 2.6–2.8 (m, 4 H); <sup>13</sup>C NMR  $\delta$  205, 161, 137, 125, 119, 37, 26; IR 1696–1731 (s), 1611 (s), 1442 (s), 1343 (s), 1217 (s), 1161 (s); mp >250 °C; MS, *m/e* 187, 186 (base), 185, 158, 157, 130; high-resolution MS, parent ion *m/e* calcd for C<sub>12</sub>H<sub>10</sub>O<sub>2</sub> 186.0681, found 186.0667.

The first emergent diketone was not further characterized but is assumed to be 22.

***s*-Hydrindacene-1,5-dione (18).** Reaction, workup, and purification were performed exactly as was described for the ring closure of *m*-benzenedipropanoic acid with *p*-benzenedipropanoic acid as the starting material. The product from the reaction had spectroscopic properties consistent with either the desired diketone 18 or the isomeric diketone *as*-hydrindacene-1,8-dione (23). Thin-layer chromatography (silica gel, CHCl<sub>2</sub>/EtOAc (1:8)) of a mixture of the product from the reaction and an authentic sample of 23 (see below) showed two clearly separated spots. Similarly, the NMR spectrum of a mixture of this reaction product and 23 showed two slightly different aromatic absorptions. This mixture melted at 110–116 °C. The product from this reaction was, therefore, identified as the desired product 18. This product was isolated in 6.0% yield (50 mg): NMR  $\delta$  7.78 (s, 2 H, Ar), 3.1–3.3 (m, 4 H), 2.6–2.8 (m, 4 H); <sup>13</sup>C NMR  $\delta$  206, 153, 142, 122, 37, 26; IR (CDCl<sub>3</sub>) 1696–1724 (s), 1442 (s), 1136 (s), 1273 (s), 1139 (s); mp 132.5–134 °C; MS, *m/e* 187, 186 (base), 185, 158, 157, 130; high-resolution MS, parent ion *m/e* calcd for C<sub>12</sub>H<sub>10</sub>O<sub>2</sub> 186.0681, found 186.0667.

***as*-Hydrindacene-1,8-dione (23).**<sup>37,38</sup> Furanocyclophane<sup>39</sup> (5,5'-ethylene-1,2-di(2-furyl)ethane) (450 mg, 2.39 mmol) was dissolved in 100 mL of MeOH to which a small portion of Rose Bengal was added. This solution was irradiated with a 650-W Sylvania sun-gun movie lamp under O<sub>2</sub> until uptake of O<sub>2</sub> ceased (3.4 h). The solution was concentrated to 20 mL, and this mixture was then stirred with a solution of 1 g of NaI in 1.5 mL of H<sub>2</sub>O and 0.5 mL of HOAc. After 1 h, Na<sub>2</sub>S<sub>2</sub>O<sub>8</sub> (saturated solution in H<sub>2</sub>O) was added until I<sub>2</sub> color disappeared. A saturated solution of Na<sub>2</sub>CO<sub>3</sub> was then added to neutralize HOAc followed by an additional 10 mL of Na<sub>2</sub>CO<sub>3</sub> solution to effect dehydration. Extraction of the resulting solution with CH<sub>2</sub>Cl<sub>2</sub> was followed by drying the organic layer over MgSO<sub>4</sub>. The solvent was removed in vacuo, yielding 334 mg (75%) of a white crystalline material. The product was purified by preparative thin-layer chromatography on silica gel with the EtOAc/CH<sub>2</sub>Cl<sub>2</sub> (10:1) solvent system, affording the desired diketone, mp 206–208.5 °C (lit. mp 208–209 °C).

**Bromination of *s*-Hydrindacene-1,7-dione 17 (Scheme IV).** A 250-mL, round-bottomed flask was charged with 500 mg (2.69 mmol) of diketone 17 which was dissolved in 100 mL of HOAc. This mixture was stirred with a magnetic stirrer and heated to 100 °C. Bromine (859 mg, 5.38 mmol) was added dropwise to the heated solution over a period of 15–20 min. The reaction was stirred an additional hour at this temperature. To the cooled solution was added CH<sub>2</sub>Cl<sub>2</sub> and H<sub>2</sub>O. After separation of the layers, the aqueous solution was extracted with CH<sub>2</sub>Cl<sub>2</sub>, and the organic portions were combined. The organic mixture was washed with 3 portions of H<sub>2</sub>O, 1 portion of saturated aqueous NaHCO<sub>3</sub>, and 1 portion of saturated aqueous NaCl and was subsequently dried over MgSO<sub>4</sub>. Evaporation of the solvent yielded a yellow crystalline material which was purified by column chromatography on silica gel with CH<sub>2</sub>Cl<sub>2</sub> solvent followed by recrystallization from EtOH (95% yield, 880 mg): NMR  $\delta$  8.25 (s, 1 H, Ar), 7.51 (s, 1 H, Ar), 4.69 (dd, 2 H, *J* = 3.2, 7.3 Hz,  $\alpha$  to ketone), 4.03 (dd, 2 H, *J* = 7.3, 19.0 Hz,  $\beta$  to ketone), 3.4 (dd, 2 H, *J* = 3.2, 19.0 Hz,  $\beta$  to ketone); IR (CDCl<sub>3</sub>) 1736 (s), 1731, 1615 (s); mp 170.0–170.5 °C; MS, *m/e* 346, 344, 342, 265 (base), 263, 184, 156, 128. Anal. Calcd for C<sub>12</sub>H<sub>8</sub>Br<sub>2</sub>O<sub>2</sub>: C, 41.90; H, 2.34. Found: C, 41.77; H, 2.40.

**$\alpha,\alpha'$ -Dibromo Diketone Ethylene Ketal 28 (Scheme IV).** In a 500-mL, round-bottomed flask was placed 1 g (2.9 mmol) of the dibromide from 17, ~4 mL of ethylene glycol, 200 mL of benzene, and a small spatula of *p*-toluenesulfonic acid. The flask was fitted with a Dean-Stark trap,

(36) Schimelpfenig, C. W. *J. Org. Chem.* **1975**, *40*, 1493.

(37) Wasserman, H. H.; Doumaux, A. R., Jr. *J. Am. Chem. Soc.* **1962**, *84*, 4611.

(38) Katz, T. J.; Balogh, V.; Schulman, J. *J. Am. Chem. Soc.* **1968**, *90*, 735.

(39) Kindly provided by Professor H. H. Wasserman.

and the reaction was heated at reflux until evolution of water had ceased (~12 days). Every few days during the course of the reaction, a small additional amount of ethylene glycol and *p*-toluenesulfonic acid was added.  $\text{CH}_2\text{Cl}_2$  was added to the cooled reaction mixture, and the organic solution was washed with 2 portions of saturated aqueous  $\text{NaHCO}_3$ , 5 portions of water, and a portion of brine and the resulting solution was dried over  $\text{MgSO}_4$ . Removal of the solvent in vacuo yielded an orange-yellow solid. This material was purified by column chromatography on silica gel by using a  $\text{CH}_2\text{Cl}_2/\text{EtOAc}$  (25:1) mixed solvent system. Recrystallization from EtOH yielded 1.13 g (90% yield) of a white crystalline solid as a mixture of isomers: NMR  $\delta$  7.37 (s, 1 H, Ar), 7.05 (s, 1 H, Ar), 4.3–4.6 (m, 2 H,  $\alpha$  to ketal), 4.1–4.3 (m, 8 H, ketal), 3.1–3.6 (m, 4 H,  $\beta$  to ketal);  $^{13}\text{C}$  NMR  $\delta$  142, 139, 121, 118, 114, 66.3, 65.9, 54, 39.3; IR ( $\text{CDCl}_3$ ) 2945 (m), 2950 (m), 2875 (m), 1425 (m), 1460 (m), 1208 (s), 1100 (s), 1025 (s); mp 183–184.5 °C; MS, *m/e* 434, 432, 430, 354, 353 (base), 352, 351; high-resolution MS, parent ion *m/e* calcd for  $\text{C}_{16}\text{H}_{16}\text{Br}_2\text{O}_4$  429.9416, found 429.9430.

**Formation of Olefin 29 (Scheme IV).** Dehydrohalogenation was carried out by dissolving 0.5 g (1.16 mmol) of **28** in refluxing MeOH (250 mL). Upon addition to this solution of methanolic KOH (prepared by dissolving 5 g of KOH in 50 mL of MeOH), the reaction mixture turned black, and refluxing was continued for 1 h. To the cooled solution was added  $\text{CH}_2\text{Cl}_2$  followed by water. Separation of the layers was followed by extraction of the aqueous layer with 2 portions of  $\text{CH}_2\text{Cl}_2$ . The combined organic layers were washed thoroughly with water and dried over  $\text{MgSO}_4$ , and the solvent was evaporated in vacuo. The resulting brown-yellow crystals could be purified by column chromatography on silica gel by using a mixed  $\text{CH}_2\text{Cl}_2/\text{EtOAc}$  (25:1) solvent system followed by recrystallization from EtOH. The yield was 90% (0.28 g): NMR  $\delta$  7.25 (s, 1 H, Ar), 6.86 (s, 1 H, Ar), 6.57 (d, 2 H,  $J$  = 5.5 Hz, vinyl), 4.1–4.3 (m, 8 H, ketal);  $^{13}\text{C}$  NMR  $\delta$  144, 142, 135, 133, 117, 116, 114, 65; IR ( $\text{CDCl}_3$ ) 2950 (m), 2880 (m), 1290 (m), 1100 (m), 1030 (m), 980 (s); mp 250 °C; MS, *m/e* 271, 270, 215, 214 (base), 186; high-resolution MS, parent ion *m/e* calcd for  $\text{C}_{16}\text{H}_{14}\text{O}_4$  270.0892, found 270.0874.

**Carbene Addition to 25 or 29 To Give 26 or 30.** In a typical reaction, 250 mg (0.9 mmol) of the olefin is dissolved in refluxing 1,1-dichloroethane. The amount of solvent used is crucial. For optimal yield, it is necessary that the reaction be run as concentrated as possible, yet most of the starting material must be in solution. Typically for a reaction this size, 6.6 mL of  $\text{CH}_2\text{CHCl}_2$  is optimal. To this refluxing solution, which should have a small amount of solid present, is slowly added 1.3 mL of BuLi (4.3 M, obtained by concentration of commercially available 2.5 M BuLi) over a period of 30 min during which time the reaction turns rust colored. The cooled solution is quenched with water and extracted with  $\text{CH}_2\text{Cl}_2$ . The organic layer is washed with water and brine and dried over  $\text{MgSO}_4$ . Evaporation of the solvent in vacuo affords a yellow-red solid. The solid is purified by preparative thin-layer chromatography on silica gel by using a mixed solvent system of  $\text{CH}_2\text{Cl}_2/\text{EtOAc}$  (24:1). Most of the fractions obtained from such a separation are still mixtures as can be seen from the NMR. The relative area of the olefinic protons at  $\delta$  6.6 and 6.1 to the bridgehead protons (bridgehead protons appear basically as doublets) at  $\delta$  2.9, 2.6, 2.3, and 2.0 can give one an idea of the ratio of starting material (and/or monocarbene adduct) to product. Yields of biscarbene addition are typically 30–40%. The mass spectrum shows a parent ion at 394 and  $M + 2$  at 396. This mixture can be used in the next step in the reaction sequence.

**Dehydrohalogenation of Carbene Adduct 30 To Give 31 (Scheme IV).** The bischloromethylcarbene adduct (200 mg, ~0.5 mmol) was dissolved in 5 mL of dimethyl sulfoxide, and the mixture was heated to 80 °C. To this was added a large excess of potassium *tert*-butoxide (sixfold excess). After 2 min, the reaction was quenched with water. This solution was continuously extracted with pentane overnight. The yellow solid obtained from evaporation of pentane can be purified by preparative thin-layer chromatography on silica gel by using  $\text{CH}_2\text{Cl}_2/\text{ether}$  (25:1). The white crystalline solid is obtained in 80% yield (163 mg) as a mixture of isomers: NMR  $\delta$  7.1 (br s, 2 H, Ar), 5.2–5.4 (m, 4 H, exocyclic methylene), 4.1–4.3 (m, 8 H, ketal), 2.8–3.1 (m, 2 H, bridgeheads), 2.4–2.6 (m, 2 H, bridgeheads);  $^{13}\text{C}$  NMR (benzene- $d_6$ )  $\delta$  146, 140, 130.5, 129, 122, 119, 117, 102.7, 102.4, 65.7, 64.8, 28.6, 28.5, 26.0, 25.8; IR ( $\text{CH}_2\text{Cl}_2$ ) 2900 (m), 1285 (s), 975 (s); mp >250 °C; MS, *m/e* 322, 251, 250, 220, 178 (base); high-resolution MS, parent ion *m/e* calcd for  $\text{C}_{20}\text{H}_{18}\text{O}_4$  322.1205, found 322.1210.

**Deketalization of 31 To Form the  $\text{C}_{20}$  Precursor 13 (Scheme IV).** To a solution of **31** (20 mg,  $6.2 \times 10^{-2}$  mmol) in tetrahydrofuran was added a small amount of 10% aqueous  $\text{H}_2\text{SO}_4$ . The mixture was stirred for 90 min at room temperature, after which it was extracted with  $\text{CH}_2\text{Cl}_2$ . The organic layer was then washed with water and brine. Subsequent drying over  $\text{MgSO}_4$  was followed by removal of the solvent in vacuo. Purification can be accomplished by preparative thin-layer chromatography

on silica gel by using  $\text{CH}_2\text{Cl}_2/\text{EtOAc}$  (24:1). The two isomers of the desired product **13** can be separated in this manner. Isomer 1: NMR  $\delta$  7.90 (s, 1 H, Ar), 7.49 (s, 1 H, Ar), 5.3–5.45 (m, 4 H, exocyclic methylene), 3.3–3.5 (m, 2 H, bridgehead), 3.05–3.2 (m, 2 H, bridgehead);  $^{13}\text{C}$  NMR  $\delta$  198.7, 157.9, 141.0, 133.1, 122.1, 120.8, 102.2, 33.5, 26.3; IR ( $\text{CDCl}_3$ , same for both isomers) 1705 (s); mp >120 °C dec; MS, (same for both isomers) *m/e* 234, 207, 206, 205, 178 (base), 177, 176; high-resolution MS (same for both isomers), parent ion *m/e* calcd for  $\text{C}_{16}\text{H}_{10}\text{O}_2$  234.0681, found 234.0666; UV (nm,  $\epsilon$ , EtOH same for both isomers) 338 (860), 278 (4800), 270 (4700), 232 (13 000). Isomer 2: NMR  $\delta$  7.90 (s, 1 H, Ar), 7.46 (s, 1 H, Ar), 5.3–5.45 (m, 4 H, exocyclic methylene), 3.3–3.45 (m, 2 H, bridgehead), 3.05–3.2 (m, 2 H, bridgehead);  $^{13}\text{C}$  NMR  $\delta$  198.7, 157.9, 141.0, 133.1, 122.1, 120.8, 120.4, 33.4, 25.8; mp >120 °C dec.

**Bromination of *s*-Hydrindacene-1,5-dione 18 (Scheme III).** Reaction, workup, and purification were performed exactly as described for the isomeric diketone **17** by using **18** as the starting material. The desired product was isolated in 93% yield (860 mg): NMR  $\delta$  7.91 (s, 2 H, Ar), 4.75 (dd, 2 H,  $J$  = 3 Hz,  $J$  = 7 Hz,  $\alpha$  to ketone), 3.95 (dd, 2 H,  $J$  = 7 Hz,  $J$  = 18 Hz,  $\beta$  to ketone), 3.4 (dd, 2 H,  $J$  = 3 Hz,  $J$  = 18 Hz,  $\beta$  to ketone);  $^{13}\text{C}$  NMR  $\delta$  198.7, 150.1, 139.2, 122.9, 43.6, 37.7; IR ( $\text{CDCl}_3$ ) 1720 (s), 1430 (m), 1125 (m); mp 189–192.5 °C; MS, *m/e* 346, 344, 342, 265 (base), 263, 184, 156, 128; high-resolution MS, parent ion *m/e* calcd for  $\text{C}_{17}\text{H}_8\text{Br}_2\text{O}_2$  341.8892, found 341.8884.

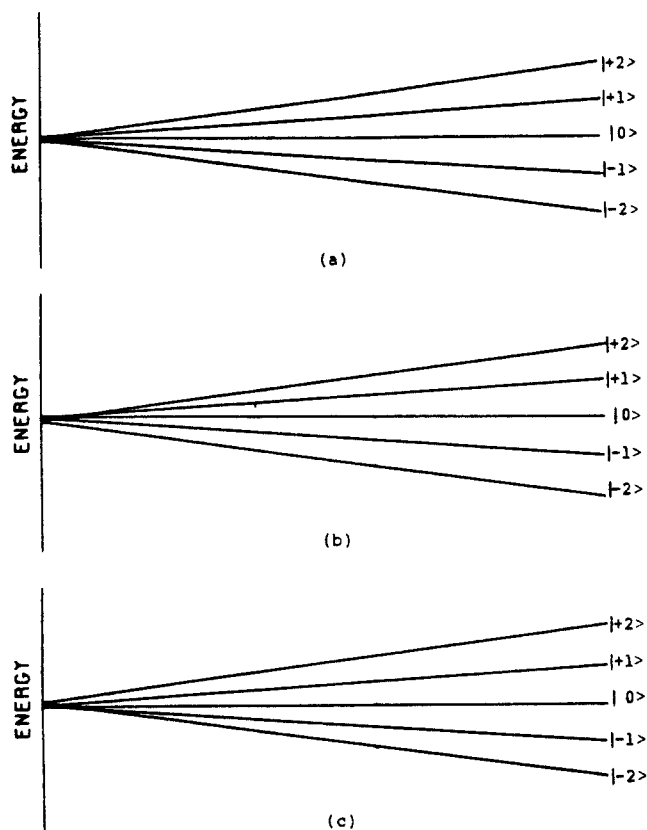
**$\alpha,\alpha'$ -Dibromo Diketone Ethylene Ketal 24 (Scheme III).** Reaction, workup, and purification were performed exactly as was described for **28** by using the dibromide from **18** as the starting material. The desired product **24** was isolated in 92% yield (1.36 g) as a mixture of isomers: NMR  $\delta$  7.19 (s, 2 H, Ar), 4.3–4.6 (m, 2 H,  $\alpha$  to ketal), 4.6–4.1 (m, 8 H, ketal), 3.0–3.6 (m, 4 H,  $\beta$  to ketal);  $^{13}\text{C}$  NMR  $\delta$  142, 140, 120, 114, 66.5, 66.1, 54.1, 53.9, 39.3; IR ( $\text{CDCl}_3$ ) 2950 (m), 2880 (m), 1425 (m), 1230 (s), 1090 (s), 1045 (s); mp 225–226 °C; MS, *m/e* 434, 432, 430, 354, 353 (base), 352, 351; high-resolution MS, parent ion *m/e* calcd for  $\text{C}_{16}\text{H}_{16}\text{Br}_2\text{O}_4$  429.9416, found 429.9392.

**Formation of Olefin 25 (Scheme III).** Reaction, workup, and purification were performed exactly as described for **28** by using **24** as the starting material. The product was isolated as a white crystalline compound in 92% yield (0.29 g): NMR  $\delta$  7.04 (s, 2 H, Ar), 6.55 (d, 2 H,  $J$  = 6 Hz, vinyl), 6.08 (d, 2 H,  $J$  = 6 Hz, vinyl), 4.0–4.3 (m, 8 H, ketal);  $^{13}\text{C}$  NMR  $\delta$  145, 141, 134, 133, 116, 114, 66; IR ( $\text{CDCl}_3$ ) 2978 (m), 2893 (m), 1041 (s); mp >250 °C; MS, *m/e* 271, 270, 215, 214 (base), 186, 158; high-resolution MS, parent ion *m/e* calcd for  $\text{C}_{16}\text{H}_{14}\text{O}_4$  270.0892, found 270.0874.

**Dehydrohalogenation of Carbene Adduct 26 To Give 27 (Scheme III).** Reaction, workup, and purification were performed exactly as was described for the dehydrohalogenation of **30** by using **26** as the starting material. The desired product was obtained as a mixture of isomers in 83% yield (136 mg): NMR  $\delta$  7.14 and 7.13 (s, 2 H, Ar), 5.2–5.4 (m, 4 H, exocyclic methylene), 4.1–4.3 (m, 8 H, ketal), 2.8–3.1 (m, 2 H, bridgeheads), 2.4–2.6 (m, 2 H, bridgeheads);  $^{13}\text{C}$  NMR  $\delta$  142.7, 142.1, 138, 119.7, 119.6, 116, 102.5, 65.9, 65.0, 27.7, 27.6, 25.5; IR ( $\text{CDCl}_3$ ) 2975 (w), 2925 (w), 2665 (m), 1275 (s), 1080 (m), 1050 (s); mp >250 °C; MS, *m/e* 322, 294, 292, 291, 264, 263, 262, 250, 220, 178 (base); high-resolution MS, parent ion *m/e* calculated for  $\text{C}_{20}\text{H}_{18}\text{O}_4$  322.1205, found 322.1200.

**Deketalization of 27 To Form the  $\text{C}_{20}$  Precursor 12 (Scheme III).** Reaction, workup, and purification were performed exactly as described for the deketalization of **31** by using **27** as the starting material. The two isomers of **12** were isolated as white crystalline compounds. Isomer 1: NMR  $\delta$  7.76 (s, 2 H, Ar), 5.28–5.4 (m, 4 H, exocyclic methylene), 3.3–3.4 (m, 2 H, bridgehead), 3.1–3.2 (m, 2 H, bridgehead).  $^{13}\text{C}$  NMR  $\delta$  197, 150.8, 141.7, 138.0, 120.8, 102.6, 33.8, 25.8; IR ( $\text{CDCl}_3$ , same for both isomers) 1690 (s) mp >120 °C dec; MS (same for both isomers), *m/e* 234, 207, 206, 205, 178 (base), 177, 176; high-resolution MS (same for both isomers), parent ion *m/e* calcd for  $\text{C}_{16}\text{H}_{10}\text{O}_2$  234.0681, found 234.0669; UV (nm,  $\epsilon$ , EtOH, same for both isomers) 314 (3500), 302 (4400), 248 (56 000). Isomer 2: NMR  $\delta$  7.65 (s, 2 H, Ar), 5.28–5.4 (m, 4 H, exocyclic methylene), 3.3–3.45 (m, 2 H, bridgehead), 3.1–3.2 (m, 2 H, bridgehead);  $^{13}\text{C}$  NMR  $\delta$  197, 150.9, 141.9, 138.0, 120.7, 102.1, 33.8, 25.8; mp >120 °C dec.

**Acetaldehyde-2,2,2- $d_3$ .**<sup>40</sup> Into a 20-mL pyrolysis tube were placed 4.46 mL of  $\text{CH}_3\text{CHO}$ , 0.64 mL of pyridine, and 14.9 mL of  $\text{D}_2\text{O}$ . The tube was sealed under vacuum and pyrolyzed at 40 °C. After 3 days the pyrolysis was complete, and the product was distilled from the solution and collected in a flask cooled with a dry ice/acetone bath. This material was resubjected to the reaction conditions for 3 days and distilled as before. The NMR spectrum showed a mixture of  $\text{CD}_3\text{CHO}$  (~95% exchanged) and paraldehyde- $d_9$  (~94% exchanged).



**Figure 11.** Energy level diagrams for a quintet with  $D = 0.01174 \text{ cm}^{-1}$ ,  $E = 0.00315 \text{ cm}^{-1}$ , and  $g = 2.0054$ . Energy is plotted on the  $y$ -axis and magnetic field on the  $x$ -axis (range 0–5000 G). Diagrams are shown for (a)  $H//x$ ; (b)  $H//y$ ; and (c)  $H//z$ .

**1,1-Dichloroethane-2,2- $d_2$ .** The mixture of  $\text{CD}_3\text{CHO}$  and paraldehyde- $d_9$  (1 mL of solution) was dissolved in 2 mL of pentane and was slowly added to a mixture of 4 g of  $\text{PCl}_5$  in 2 mL of pentane in a 25-mL, round-bottomed flask fitted with a reflux condenser. After addition was complete, the reaction mixture was stirred for 30 min and slowly quenched with water. Separation of the layers was followed by extraction of the aqueous layer with 5 mL of pentane. The combined organic layers were subsequently dried over a small amount of  $\text{MgSO}_4$  and filtered. The filtrate was purified by VPC by using a 10 ft  $\times$   $3/8$  in. 5% carbowax column at 70 °C to afford  $\text{CD}_3\text{CHCl}_2$  (92% incorporation as determined by NMR). This deuterated carbene precursor was used in place of  $\text{CH}_3\text{CHCl}_2$  to repeat Scheme III and form **12- $d_4$** . The NMR spectrum of the latter substance showed very little absorption in the  $\delta$  5.28–5.4 region.

**Standard Procedures. EPR Spectroscopy.** The sample was prepared by dissolving 1–5 mg of the precursor in the appropriate solvent and placing the mixture into a reusable EPR tube. This tube was composed of  $\sim 30$  mm long quartz tubing (4 mm o.d.) connected to a length of Pyrex tubing of the same diameter. The sample was subjected to 3 freeze–pump–thaw cycles after which it was sealed while frozen under vacuum. The sample was then placed in the cavity of the EPR spectrometer and photolyzed as described. The glass filters used were Oriel Corp. No. 5182 ( $305 \text{ nm} \leq \lambda \leq 525 \text{ nm}$ ) and Oriel Corp. No. 5148 ( $\lambda > 425 \text{ nm}$ ). To prevent overheating of the filters a stream of  $\text{N}_2$  gas was passed over the filter during photolysis.

**Curie Studies.** The photolysis was carried out at a temperature where all signals are stable ( $< 50 \text{ K}$ ). The temperature was then lowered at regular intervals. A spectrum was recorded at  $\sim 5$ – $10^\circ$  intervals until the lowest temperature obtainable was reached. The temperature was then raised in the same manner while recording spectra at regular intervals until the high-temperature limit was reached (this temperature was sample dependent and was determined earlier). This process was repeated until a sufficient number of spectra had been collected. The relative area under the curve was taken as being proportional to the peak-to-peak heights for those peaks, since the line shape does not change with temperature.

**Intensity Studies.** The sample was photolyzed (36–50 K) through Oriel filter 5182 for the time specified in the Results and Discussion section ( $\sim 30 \text{ s}$ ) to produce the primary biradical. The spectrum was collected, and the exact temperature was noted. Photolysis was then

continued through Oriel filter 5148 to form the secondary photoproduct. At several points during the photolysis, spectra were collected digitally. Before collecting spectra, photolysis was interrupted and the temperature was adjusted to ensure the same temperature as was noted during collection of the first spectrum. After completion of photolysis, the spectra were integrated by using a computer program INTEG.FOR as described elsewhere.<sup>41</sup> Under these conditions, saturation was not a factor at the microwave power levels used (0.02–0.05 mW).

**UV-vis spectroscopy** at cryogenic temperatures was carried out with an Air Products Displex cryostatic closed-cycle helium refrigerator, using quartz or Suprasil outer windows on the spectroscopic shroud. Details are reported elsewhere.<sup>42</sup>

**Theoretical Calculations.** The INDO/S-CI program we used is an updated version of the Ridley–Zerner one<sup>43</sup> and has been described elsewhere.<sup>14</sup> We thank M. Zerner for making it available to us. All the parameters were those provided except for  $f_{\text{ppr}}$ , which was adjusted to a value of 0.615 (instead of the standard 0.680). This value was chosen to fit the observed spectrum of 1,3-perinaphthadiyl triplet.<sup>31a</sup> For calculations on triplet species, triplet-restricted open-shell Hartree–Fock orbitals (ROHF) were used with idealized geometries and singly excited configurations only. For the quintet, triplet parameters were used to carry out quintet ROHF MO calculations, and single excitation CI was carried out on this orbital set. The INDO/S-CI results are presented in bar form on the spectra. PPP-CI simulations also were carried out as a comparison technique, by using the TRIBBLE package available on the Yale University Department of Chemistry VAX 11/750 computer. Details of both of the methods and numerical listings of the results are given elsewhere.<sup>42</sup>

**Acknowledgment.** This research was supported in part by the National Science Foundation and the National Institutes of Health. We also thank the Dox Foundation for a fellowship (to D.E.S.), F. Hund, M. Zerner, W. T. Borden, J. M. McBride, R. J. Cross, and R. Merrill for help on various aspects of this work, and the University of Connecticut Department of Computer systems for a generous grant of computer time.

#### Appendix A. Statistical Intensity Factor in Multispin EPR Spectroscopy

In multispin systems, two samples containing equal total numbers of unpaired electrons, nevertheless, will have different EPR spectroscopic signal intensities, if their spins arise from states of different multiplicity. This fact was first pointed out to us by McBride<sup>44</sup> and, as far as we can determine, is not mentioned in the didactic literature. The origin and choice of the correct statistical factor to apply are readily demonstrated.

The probability of an “allowed” ( $\Delta m_s = \pm 1$ ) EPR transition is proportional to  $\Delta N$ , the population difference between adjacent sublevels of the paramagnetic state involved in the transition.<sup>45</sup> For any two sublevels, the ratio of populations in the higher and lower sublevels is given by a Boltzmann relationship (eq A1),

$$(N_{\text{higher}}/N_{\text{lower}}) = e^{-\Delta E/RT} = e^{-g\beta H_z/RT} \quad (\text{A1})$$

where  $\Delta E$  is the energy separation,  $g$  is the electronic  $g$ -factor appropriate to the paramagnetic species, and the other terms have their usual meaning.

Suppose we wish to obtain the statistical factor for comparison of the signal intensity of a triplet species with that of two doublets. Let  $N_T$  be the total number of unpaired electrons in the triplet sample and  $N_D$  be the total number in the two-doublet sample. The energy gap between sublevels at the usual magnetic field strength is very small compared to  $RT$  at most experimental temperatures. For example, a typical sublevel spacing of about  $0.1 \text{ cm}^{-1}$  corresponds to about  $0.3 \text{ cal/mol}$ , and the temperature would have to be lowered below  $15 \text{ K}$  in order for the population ratio of eq A1 to differ from unity by more than 1%. Accordingly, under most circumstances of interest in the present context, the

(41) Seeger, D. E. Ph.D. Dissertation, Yale University, 1983, p 166ff.

(42) Lahti, P. M. Ph.D. Dissertation, Yale University, 1985, p 369ff.

(43) (a) Ridley, J.; Zerner, M. *Theor. Chim. Acta* **1973**, *32*, 11. (b) Ridley, J.; Zerner, M. *Ibid.* **1976**, *42*, 233.

(44) (a) McBride, J. M., personal communication, as cited by: Platz, M. S.; Berson, J. A. *J. Am. Chem. Soc.* **1980**, *102*, 2358. (b) See also ref 13.

(45) See: Carrington, A.; McLachlan, A. D. “Introduction to Magnetic Resonance”; Harper and Row: New York, 1967; p 5.

spins will be evenly distributed over the sublevels to a very good approximation (eq A2 and A3).

$$N_T = N_{+1} + N_0 + N_{-1} \approx \frac{N_T}{3} + \frac{N_T}{3} + \frac{N_T}{3} \quad (\text{A2})$$

$N_{2D} =$

$$N_{+1/2} + N_{-1/2} + N_{-1/2} + N_{-1/2} \approx \frac{N_{2D}}{4} + \frac{N_{2D}}{4} + \frac{N_{2D}}{4} + \frac{N_{2D}}{4} \quad (\text{A3})$$

The population differences are given by eq A4 and A5, which are derived from eq A1-A3.

$$\Delta N_T = N_{+1} - N_0 = N_0(e^{-g\tau\beta H_i/RT} - 1) = \frac{N_T}{3}(e^{-g\tau\beta H_i/RT} - 1) \quad (\text{A4})$$

$$\Delta N_{2D} = N_{+1/2} - N_{-1/2} = N_{-1/2}(e^{-g_{2D}\beta H_i/RT} - 1) = \frac{N_{2D}}{4}(e^{-g_{2D}\beta H_i/RT} - 1) \quad (\text{A5})$$

The relative probability of a one-quantum transition is given by the ratio of the right-hand sides of eq A4 and A5 (eq A6).

$$\frac{\Delta N_T}{\Delta N_{2D}} = \text{relative probability} = \frac{4}{3} \frac{N_T(e^{-g\tau\beta H_i/RT} - 1)}{N_{2D}(e^{-g_{2D}\beta H_i/RT} - 1)} \quad (\text{A6})$$

Since the *g*-factors for structurally similar paramagnetic species are likely to be nearly equal, the terms in parentheses in eq A6 cancel, and if  $N_T = N_{2D}$ , the relative probability is  $4/3$ , that is, the intensity of the spectrum of a triplet species is inherently  $4/3$  that of an equal number of spins in two doublets. By a similar argument, it can be shown that the statistical factor  $\Delta N_Q/\Delta N_{2T} = 6/5$  for the quintet vs. two triplets case.

#### Appendix B. Fit of the EPR Spectrum of 15 to a Quintet Hamiltonian

The spin matrices  $S_x$ ,  $S_y$ , and  $S_z$  and their squares needed for the solution of eq 4 for a quintet are constructed from the quintet basis functions  $\langle -2|$ ,  $\langle -1|$ ,  $\langle 0|$ ,  $\langle +1|$ , and  $\langle +2|$  by using the spin equations.<sup>24</sup> Their explicit form is given elsewhere.<sup>46a</sup> Substitution into the Hamiltonian (eq 4) and conversion to matrix form gives the quintet Hamiltonian matrix,<sup>46b</sup> which is then diagonalized to yield the eigenvalues and eigenvectors. The  $\Delta m_s = \pm 1$  transitions are found by matching the energy gap between adjacent quintet sublevels with the microwave energy. The simulation process is

facilitated by a computer program, QUINTET.FOR, written by one of us (D.E.S.) and listed elsewhere.<sup>46c</sup>

All of the input for this program is taken from the default file FOR007.DAT which is created from the program QNTDAT.FOR. The numbers in this file consist of the microwave frequency, *D*, *E*, *g*, and the magnetic field range over which the eigenvalues are to be calculated. These parameters are filled into the Hamiltonian matrix<sup>46b</sup> which is then diagonalized<sup>47</sup> at regular intervals (specified by the user) over the magnetic field range. This diagonalization is carried out for each of the three canonical orientations. If desired, the program will then search for the positions of possible absorptions. It does this by searching for minima in the function of the type

$$F(E', E'') = |\delta - (E' - E'')|$$

where  $E'$  and  $E''$  are any two eigenvalues and  $\delta = h\nu$ . A minimum will occur in the function whenever  $\delta \approx E' - E''$  and a transition is possible. Finally, the program QNTPLT.FOR can plot out the eigenvalues as a function of magnetic field to obtain the energy level diagram at each of the canonical orientations for the given values of *D*, *E*, and *g*. To verify that the program was running correctly, we successfully reproduced the energy level diagrams that were published by Dowsing.<sup>24b</sup>

To save computer time, one proceeds as follows when simulating a spectrum. For a given value of *D* and *E* (these can be estimated by inspection of the positions of the two highest field transitions in the spectrum, see eq 2 and 3), the energy level diagrams are plotted over a large magnetic field range (e.g., 0-5000 G). Typically, if the eigenvalues are determined every 100 G, fairly accurate diagrams are produced. From these diagrams, one can estimate the range of magnetic fields over which a desired transition (e.g.,  $\Delta m_s = 1$ ) will occur. One then recalculates the eigenvalues over this narrow range by using smaller intervals of magnetic field (e.g.,  $\sim 1$  G) and searches for transitions (the value of the interval chosen depends upon the accuracy desired for the resonant fields). The positions of the absorptions are printed into FOR010.DAT. One then varies the ZFS parameters until the positions of the calculated transitions adequately simulate the experimental ones. Note that the simulation here deals only with line positions, not intensities.

Figure 11 shows the energy level diagrams for the canonical orientations with the "best fit" values of *D*, *E*, and *g*, which were obtained by varying these parameters to match the two highest field transitions. The fit is shown in Figure 2 and listed in Table I.

(46) Seeger, D. E. Ph.D. Dissertation, Yale University, New Haven, CT; (a) p 112; (b) p 113; (c) p 251.

(47) We thank Professor R. J. Cross for making a diagonalization sub-routine available to us.

## 8,8'-Bibicyclo[3.2.1]octylidene Radical Cation

Stephen F. Nelsen\* and Daniel L. Kapp

Contribution from the S. M. McElvain Laboratories of Organic Chemistry, Department of Chemistry, University of Wisconsin, Madison, Wisconsin 53706. Received September 9, 1985

**Abstract:** *syn*-8,8'-Bibicyclo[3.2.1]octylidene cation radical (*syn*-8<sup>+</sup>) has a rotational barrier about its central C-C bond which is above 15.4 kcal/mol. Oxygenation of *syn*-8 under catalytic cation radical conditions at -78 °C gives only the dioxetane with oxygens equatorial to both six-membered rings (**20ee**). Oxygenation of *anti*-8 gives an 80:20 mixture of **20ea**:**20ee**. These results are interpreted as indicating an open  $\beta$ -peroxy radical carbenium ion in the oxygenation reaction and a stereoselectivity for attack anti to the three-carbon bridge in both the addition of oxygen to the olefin cation and closure of the open intermediate.

One-electron oxidants, including tris(*p*-bromophenyl)ammonium hexachloroantimonate,<sup>1,2</sup> photoexcited dicyanoanthracene,<sup>3,4</sup>

nitrosyl cation,<sup>2</sup> and electrochemical oxidation,<sup>4,5</sup> catalytically convert oxygen and biadamantylidene (**1**) to its dioxetane, **2**. The